JAMES | Journal of Advances in Modeling Earth Systems

RESEARCH ARTICLE
10.1029/2023MS003689

Nutrient Dynamics in a Coupled Terrestrial Biosphere and Land Model (ELM-FATES-CNP)

Ryan G. Knox[1], Charles D. Koven[1], William J. Riley[1], Anthony P. Walker[2], S. Joseph Wright[3], Jennifer A. Holm[1], Xinyuan Wei[2], Rosie A. Fisher[4], Qing Zhu[1], Jinyun Tang[1], Daniel M. Ricciuto[2], Jacquelyn K. Shuman[5], Xiaojuan Yang[2], Lara M. Kueppers[1,6], and Jeffrey Q. Chambers[1,6]

[1]Lawrence Berkeley National Laboratory, Berkeley, CA, USA, [2]Oak Ridge National Laboratory, Oak Ridge, TN, USA, [3]Smithsonian Tropical Research Institute, Ancon, Panama, [4]CICERO Center for International Climate Research, Oslo, Norway, [5]Now at NASA Ames Research Center, National Center for Atmospheric Research, Boulder, CO, USA, [6]University of California, Berkeley, CA, USA

Key Points:

- The nutrient enabled ELM-FATES model represents expected pattern responses to nutrient availability and parameter perturbations
- The model has been designed to introduce a reasonably small parameterization burden
- These hypothesis can capture some but not all elements of carbon-nutrient dynamics and can be further inter-compared with other hypotheses

Supporting Information:

Supporting Information may be found in the online version of this article.

Correspondence to:

R. G. Knox,
rgknox@lbl.gov

Citation:

Knox, R. G., Koven, C. D., Riley, W. J., Walker, A. P., Wright, S. J., Holm, J. A., et al. (2024). Nutrient dynamics in a coupled terrestrial biosphere and land model (ELM-FATES-CNP). *Journal of Advances in Modeling Earth Systems*, *16*, e2023MS003689. https://doi.org/10.1029/2023MS003689

Received 2 MAR 2023
Accepted 2 JAN 2024

Author Contributions:

Conceptualization: Ryan G. Knox, Charles D. Koven, William J. Riley, Anthony P. Walker, Jennifer A. Holm, Rosie A. Fisher, Qing Zhu, Jinyun Tang, Daniel M. Ricciuto, Xiaojuan Yang, Lara M. Kueppers, Jeffrey Q. Chambers

Abstract We present a representation of nitrogen and phosphorus cycling in the Functionally Assembled Terrestrial Ecosystem Simulator, a demographic vegetation model within the Energy Exascale Earth System land model. This representation is modular, and designed to allow testing of multiple hypothetical approaches for carbon-nutrient coupling in plants. Novel model hypotheses introduced in this work include, (a) the controls on plant acquisition of aqueous mineralized nutrients in the soil and (b) fairly straight forward methods of allocating nutrients to specific plant organs and their losses through live plant turnover as well as litter fluxes generated through plant mortality. This combines the new with pre-existing hypotheses (such as nitrogen fixation and soil decomposition) into a system that can accommodate plant-soil dynamics for a large number of size- and functional-type-resolved plant cohorts within a time-since-disturbance-resolved ecosystem. Root uptake of nutrients is governed by fine root biomass, and plants vary in their fine root biomass allocation in order to balance carbon and nutrient limitations to growth. We test the sensitivity of the model to a wide range of parameter variations and structural representations, and in the context of observations at Barro Colorado Island, Panama. A key model prediction is that plants in the high-light-availability canopy positions allocate more carbon to fine roots than plants in low-light understory environments, given the widely different carbon versus nutrient constraints of these two niches within a given ecosystem. This model provides a basis for exploring carbon-nutrient coupling with vegetation demography within Earth system models.

Plain Language Summary This work introduces a new set of nutrient cycling hypotheses incorporated into a terrestrial biosphere model. This includes the cycling of carbon, nitrogen and phosphorus, and focuses mainly on plant acquisition, allocation, and turnover. An analysis shows the model offers reasonable responses to perturbations in parameter constants and variability in climate forcing, considering its design balance between process complexity and parameterization burden.

1. Introduction

Projections of the global climate system response to anthropogenic CO_2 emissions require coupled models of the climate system and carbon cycle. Much of the uncertainty in current climate projections arises from the global terrestrial carbon cycle, and in particular the responses of plants to elevated CO_2 (Arora et al., 2020). Many current Earth System Models (ESMs) do not take into account plant size structure, disturbance history, and other aspects known to govern ecosystem function and thereby current and future responses to anthropogenic pressures (D. Purves & Pacala, 2008). Additionally, limitation by nutrients of plant productivity under elevated CO_2 has been shown to strongly affect both the historical and future uptake of carbon (Hungate et al., 2003; P. Thornton et al., 2007; Zaehle & Friend, 2010; Wang et al., 2015). The importance of including nutrient dynamics in projecting the global terrestrial carbon budget is evidenced by its expanded role in Earth System land models, such as CASACNP (Wang et al., 2010), GFDL LM4.1-BNF (Kou-Giesbrecht et al., 2021; Sulman et al., 2019), LPJ-GUESS (Dantas de Paula et al., 2021; Smith et al., 2014), ED2-MEND-NCOM (Medvigy et al., 2019), and Quincy v1.0 (Thum et al., 2019) to name a few. Also, the land model for the Energy Exascale Earth System Model (E3SM) (Caldwell et al., 2019), the ESM used in this research, has been coupled with the FUN nutrient cycling model (carbon, nitrogen and phosphorus) using its big-leaf representation of vegetation (Allen et al., 2020;

Data curation: S. Joseph Wright
Formal analysis: Ryan G. Knox, Charles D. Koven, William J. Riley, Anthony P. Walker, S. Joseph Wright, Xinyuan Wei, Lara M. Kueppers
Investigation: Ryan G. Knox, Charles D. Koven, William J. Riley, Anthony P. Walker, S. Joseph Wright, Jennifer A. Holm, Xinyuan Wei, Qing Zhu, Jinyun Tang, Daniel M. Ricciuto, Xiaojuan Yang, Lara M. Kueppers, Jeffrey Q. Chambers
Methodology: Ryan G. Knox, Charles D. Koven, William J. Riley, Anthony P. Walker, Qing Zhu
Resources: S. Joseph Wright
Software: Ryan G. Knox, Jennifer A. Holm, Xinyuan Wei, Jacquelyn K. Shuman
Validation: Ryan G. Knox, S. Joseph Wright, Xinyuan Wei
Writing – original draft: Ryan G. Knox, Charles D. Koven
Writing – review & editing: Ryan G. Knox, Charles D. Koven, William J. Riley, Anthony P. Walker, S. Joseph Wright, Jennifer A. Holm, Xinyuan Wei, Rosie A. Fisher, Qing Zhu, Jinyun Tang, Xiaojuan Yang, Lara M. Kueppers

Braghiere et al., 2022; Brzostek et al., 2014; J. Fisher et al., 2010). Despite their importance, processes that govern nutrient cycling rates in ecosystems are highly uncertain, since many of them occur belowground where observation is more difficult than in plant canopies. To allow exploration of this epistemic uncertainty, we propose here a modular approach to representing nutrient cycling that facilitates exploration of alternative process hypotheses and parameter and structural uncertainty quantification.

This manuscript describes a modeling methodology and new science hypotheses explicitly and only for plant acquisition, storage, and allocation of nutrients within the terrestrial biosphere of an ESM. No fundamentally new modeling and science hypotheses are introduced to soil biogeochemistry or nitrogen fixation. We acknowledge that nutrient limitations have been incorporated in other terrestrial biosphere models that use individual based vegetation concepts (see above paragraph for several examples). The specific acquisition and allocation methods explained here differ from those mentioned. The different implementations here and in other terrestrial biosphere models are hypotheses, because they tentative assumptions that attempt to represent massively complex natural process with numerical representations tuned by parameter constants. It is crucial that ESMs explore different representations to evaluate these hypotheses and ultimately inter-compare for fidelity with observations.

While this manuscript leverages existing hypotheses for in-soil competition between plants, microbes and minerals, the previous coupling in ELM of plant-soil nutrient exchange had only been performed with the "big-leaf" (i.e., a model that lacks size structure and demography) vegetation model, and has thus required us to reformulate the existing soil nutrient competition schemes to work with the Functionally Assembled Terrestrial Ecosystem Simulator (FATES) individually based vegetation model. So this manuscript also describes how the plant nutrient dynamics interface with existing soil nutrient hypotheses, but does not introduce new soil modeling hypotheses.

This system is an extension of the coupled modeling framework of the E3SM model (Caldwell et al., 2019) and the FATES. E3SM includes a land model (ELM) among other components such as atmosphere, ocean, ice, and human. The terrestrial vegetation simulated in FATES is based on the plant size and time-since-disturbance structured approach derived from the Ecosystem Demography model (R. A. Fisher et al., 2015; Moorcroft et al., 2001).

The nutrient modeling framework we describe here can be summarized in four model components: (a) a new module that handles the nutrient and carbon allocations to different organs within the plant, designated the Plant Allocation, Reactions, and Transport Extensible Hypotheses (PARTEH), (b) the tracking of various chemical elements (which previously was limited to carbon) in seed, unfragmented litter, and coarse woody debris pools, (c) a means of acquisition and competition for nutrients by FATES plants amongst microbes and mineral surfaces and (d) the integration of a pre-existing symbiotic nitrogen fixation scheme into the FATES framework. An evaluation of the model at a tropical test-bed site follows. This expanded version of the model will be referred to as ELM-FATES-CNP (where CNP simply refers to "C"arbon "N"itrogen and "P"hosphorus). Shorthand notations of C, N and P may be used in this manuscript to reference non-specific forms of Carbon, Nitrogen and Phosphorus respectively.

2. Model Description–Plant-Soil Nutrient Dynamics

The ELM model (Burrows et al., 2020) resolves numerous processes related to the cycling of water, energy, carbon, nitrogen and phosphorus in natural and anthropogenic ecosystems. Soil decomposition (in the simulations of this manuscript) is handled via a derivative of the CENTURY approach (C. Koven et al., 2013; Parton et al., 1988). Other decomposition modules are available in ELM and the Community Land Model (CLM) (Lawrence et al., 2020), such as the Converging Trophic Cascade (P. E. Thornton & Rosenbloom, 2005; P. Thornton et al., 2007; P. E. Thornton et al., 2009) and the MIcrobial-MIneral Carbon Stabilization with Carbon and Nitrogen (Kyker-Snowman et al., 2020; W. R. Wieder et al., 2019). The former is compatible with FATES-CNP. The latter is half-way through the process of compatibility as of this writing. In all of these decomposition models, all prognostic carbon and nutrient pools native to these schemes are maintained when coupled with FATES nutrient cycling. Total ecosystem nitrogen fixation has been represented in ELM by assuming proportionality with either evapotranspiration or net primary productivity (Cleveland et al., 1999; P. Thornton et al., 2007). Symbiotic fixation at the plant level is introduced in the Methods section and will be described in more detail. When symbiotic fixation is represented by FATES, the total ecosystem fixation module in ELM is scaled down to represent only free-living fixation in the soil. Soil biogeochemical dynamics lead nutrients to cascade from organic pools with different turnover times to ammonium (NH_4), nitrate (NO_3), and phosphate (PO_4) pools through organic matter mineralization processes. Soil inorganic nutrients are dynamically maintained

as a result of supply fluxes (e.g., deposition, net mineralization, nitrogenase/phosphatase activities) and consumption fluxes (e.g., plant uptake, leaching loss). The deposition of nutrients is provided by external data sets (Mahowald et al., 2008). Unlike phosphorus, the input of nitrogen deposition to the system is somewhat obscured because of the much larger fixation fluxes. Unlike inorganic nitrogen, soil inorganic phosphorus is also affected by mineral surface interactions via adsorption, and occlusion. The former is reversible process that quickly equilibrates phosphate between soil solution and adsorbed pool at mineral surface, while the latter is a slow and irreversible process to remove available phosphate. ELM contains two alternative representations of competition for these nutrient species amongst plants, microbes (decomposers for organic pools, as well as nitrifiers and denitrifiers for mineral nitrogen pools), and mineral surfaces (for phosphorus). These are the Relative Demand (RD) approach (P. Thornton et al., 2007; X. Yang et al., 2014, 2019) and a Capacitance-Based approach that applies the Equilibrium Chemistry Approximation (CB) (Tang & Riley, 2013; Zhu et al., 2016, 2019).

FATES is a vegetation demography model (R. A. Fisher et al., 2015; C. D. Koven et al., 2020) that represents the demographics of vegetation using plant size and time-since-disturbance structured scaling algorithms defined in the Ecosystem Demography (ED) Model (Moorcroft et al., 2001). FATES represents vegetation by grouping plants of similar size and functional type into cohorts, which inhabit patches of the landscape that are defined by their time since last disturbance. Unlike unstructured vegetation models, which treat growth and mortality processes as changes to the size of whole ecosystem-level carbon and nutrient pools, cohort-based vegetation models like FATES explicitly track the growth of plants, the size (volume, height, etc) growth of various components, and the resulting carbon and nutrient pools of their tissues using allometrically defined scaling relationships with stem diameter. FATES also allows for competition for light between plant types in the same vertical profile, which leads to self-thinning dynamics and other spatio-temporal changes in vegetation composition to emerge as a function of variation in plant functional traits. FATES estimates mortality at the plant cohort scale, based on several factors including carbon starvation, understory impact survival, hydraulic stress (R. A. Fisher et al., 2015), background mortality (i.e., unspecified or unknown effects) (Moorcroft et al., 2001), fire (Thonicke et al., 2010), and relationships with plant age or size (Needham et al., 2020). In the current version of FATES, the time-since-disturbance patch discretization only resolves heterogeneity in the above-ground environment, with all cohorts on all patches drawing water and nutrients from the same soil pools.

FATES represents a variety of processes, including but not limited to: photosynthesis and its coupling with water limitations on stomatal conductance (G. Bonan et al., 2014; Collatz et al., 1991; Farquhar et al., 1980; Oleson et al., 2013), respiration (Ryan, 1991) of live tissues, vertical distribution of canopy functional trait parameters (G. B. Bonan et al., 2012), radiation scattering (Norman, 1979), phenology (Botta et al., 2000), and turnover into coarse woody debris and fine litter (R. A. Fisher et al., 2015; Oleson et al., 2013). In this model, the organ nutrient concentrations (i.e., stoichiometry) are time-invariant constants $\alpha_{(o,N)}$. This is assumed to be a plant trait, that is reflective of the mean nutrient content for the functional type or group of the plant. Plant maintenance respiration rates (Ryan, 1991) are calculated for each organ and are sensitive to the nitrogen concentrations. Photosynthesis rates are also regulated by time-invariant plant traits, including the maximum carboxylation rate of rubisco V_{cmax}, which is assumed to be a trait positively correlated with the nutrient concentrations of the leaves. The reasoning and implications of constant stoichiometry assumptions in this modeling implementation are discussed in Section 4.4.

Cohort and ecosystem scale photosynthesis and respiration rates are influenced via growth and allocation response to nutrient availability and its effect on biomass of resource acquiring organs. Nutrient concentrations regulate plant growth through the construction costs to build tissues. FATES' radiation scattering module accounts for both the vertical structure of vegetation and the variable scattering characteristics of different plant functional groups in parallel (R. A. Fisher et al., 2015). The spatial configuration of the canopy scattering elements is driven by a modified perfect plasticity approximation (R. A. Fisher et al., 2015; C. D. Koven et al., 2020; D. W. Purves et al., 2008). While FATES can optionally utilize sophisticated representations of plant hydraulics (Christoffersen et al., 2014; Fang et al., 2022; Fyllas et al., 2014) and fire (Buotte et al., 2021; Ma et al., 2021; Thonicke et al., 2010), in order to focus on nutrient dynamics, these options were not active in the modeling exercises described herein. Details on all of these process representations can be found in the FATES technical documentation (FATES-Development-Team, 2019).

The introduction of nutrients to FATES, via the PARTEH approach to (Plant Resource Allocations, Reactions, and Transport Extensible Hypotheses) described here, follows a sequence of operations that are shown in

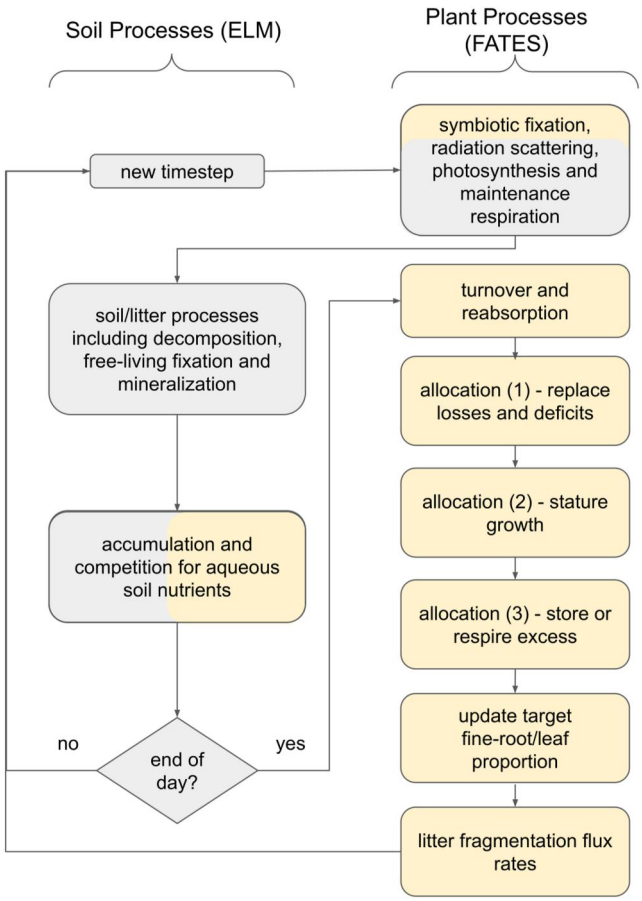

Figure 1. Flow-chart of key processes and order of operations for nutrient cycling in ELM-FATES-CNP. This chart places more emphasis on plant-side processes. New processes described in this manuscript are shown in yellow boxes. Gray boxes indicate pre-existing but relevant processes in the model. For the process of soil nutrient competition, nothing has changed from the original schemes, except how plants present themselves as competitors (shown as with a split gray/yellow color). In the box highlighting symbiotic fixation, scattering, etc., symbiotic fixation is a new process and the others are un-modified.

Figure 1. The descriptions of these processes follow the flow-chart order and can be found in the following subsections: symbiotic fixation in 2.1, plant acquisition of aqueous soil nutrients in 2.2, retranslocation during senescent turnover in 2.3, updating the target fine-root biomass (the optimal fine-root biomass associated with the plant's nutrient requirements) in 2.6, and allocation to the various plant organs in 2.5. Soil hydrology in ELM is the same as that described in the CLM technical manual (Oleson et al., 2013).

An overview of the nutrient mass fluxes through the key nutrient pools in the soil-plant system are shown in Figure 2. Also, a list of all variables and parameters described in this manuscript are provided in Appendix A Table A1.

Three chemical elements are tracked and conserved by mass within the plant, litter and soil system: carbon (non isotope specific), nitrogen, and phosphorus. The masses of these elements at any given instance in time are designated $C_{(o)}$ for carbon and $M_{(o,s)}$ for the two nutrients elements, where o is the generic subscript for the organs and s is the generic subscript for the two nutrient elements nitrogen and phosphorus.

Parameter constants are indicated by lowercase Greek letters. Some variables not associated with a mass use lower-case letters. Unless specified otherwise, fluxes and rates of change use an over-dot (i.e., $\dot{X}$). All plant states have units of [kg plant^{-1}]. Turnover and allocation within the plant occur at a daily frequency. Thus, they have units of [kg plant^{-1} day^{-1}]. Nutrient competition between plants and soil competitors (e.g., microbes, mineral surfaces) is resolved at sub-diurnal timescales (typically 30 min), and is integrated over the day and presented as a daily uptake [kg plant^{-1} day^{-1}].

Each plant cohort is represented by an average individual that maintains discrete mass pools for the following organs (and associated sub-scripts): leaf (*lf*), sap-wood (*sa*), dead-wood (*de*), fine-root (*fr*), reproductive (*re*) and storage (*so*). Sapwood refers to all living woody tissues, including organs such as the cambium, phloem, and xylem. Dead-wood refers to all non-living tissues such as heartwood and bark. Both cases (dead and live) include below and above-ground components. The dead pool should not be confused with the coarse woody debris associated with dead trees. Fine-roots are functionally classified as tissues with high turnover and respiration rates, as compared to below-ground sapwood (coarse roots). Reproductive organs encompass all ephemeral tissues associated with reproduction, including seeds, cones, flowers, fruits, etc. For storage, the term "organ" is used loosely because reserves are spatially distributed throughout the plant, often in vacuoles, referring to all forms of C, N, and P that can be re-mobilized for growth or maintenance of other tissues. Carbon storage refers to non-structural carbohydrates of starches and sugars. Storage of N is often comprised of proteins and amino compounds (Millard & Grelet, 2010), whereas phosphate compounds are typical for phosphorus storage (S.-Y. Yang et al., 2017).

Plants represented in FATES-CNP can acquire nutrients through several means: (a) uptake of mineral nutrients from soil solution, (b) symbiotic nitrogen fixation, and (c) retranslocation preceding litterfall. The model design is modular and interchangeable with alternative hypotheses. Here we describe the default options for these uptake processes.

2.1. Acquisition Through Symbiotic Fixation

The carbon cost of symbiotic nitrogen fixation is modeled as an obligate (temperature dependent) increase in maintenance respiration (Houlton et al., 2008). Plants that are designated as nitrogen fixers generate a fixation rate $\dot{M}_f$ [kgN plant^{-1} day^{-1}] by respiring carbon r_f [kgC plant^{-1} s^{-1}] at a rate that is a constant fraction $\rho_{f(\mathrm{pft})}$ of all non-fixation fine-root maintenance respiration (Ryan, 1991) (non-growth) costs r_m [kgC plant^{-1} s^{-1}]. This simplification assumes that all resources driving nitrogen fixation are mediated through respiration, and those costs act

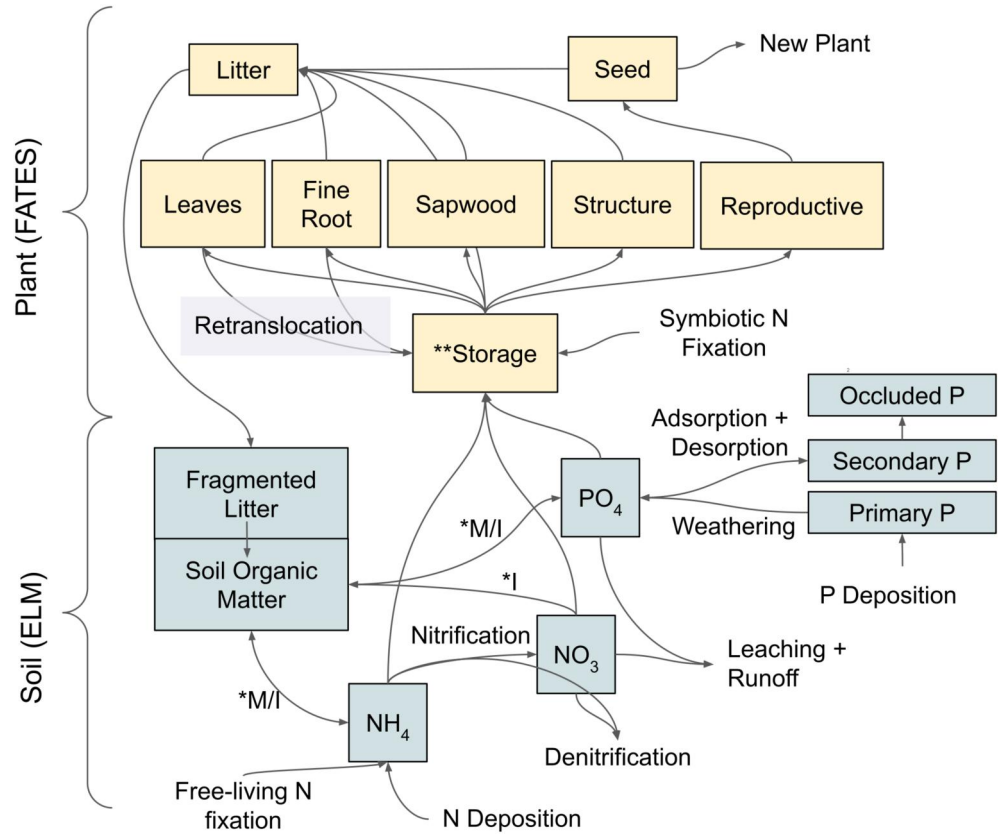

Figure 2. Diagram showing the key pools and fluxes for nitrogen and phosphorus cycling in ELM-FATES-CNP. Plant pools are shown with yellow boxes, soil pools are shown with slate colored boxes. *I and M are short-hand for (I)mmobilization and (M)ineralization fluxes. **Denotes the special status of nutrient storage, in that storage nutrient pools are distinct from the carbon storage pool. The leaf, fine-root, sapwood, structure and reproductive tissues assume that carbon, nitrogen and phosphorus are bound together in the tissues. Leaching refers to phosphate and nitrate (not ammonium) and denitrification losses are from both nitrate and from instantaneous conversion following nitrification. Note that the senescent tissues of functionally assembled terrestrial ecosystem simulator plants, either from turnover on live plants, or through the death of plants, does transfer to the soil organic pool, via the litter pools.

as a surrogate for other costs such as building and maintaining nodules and feeding specialized bacteria. This represents an obligate strategy because all plants of a Plant Functional Type (PFT) with a nonzero value of $\rho_{f(\mathrm{pft})}$ constantly fix N and incur the respiratory cost of doing so. The representation of facultative nitrogen fixation strategies in FATES is left for future work. The nitrogen fixation flux is accumulated on each sub-daily time-step (of duration $\Delta t = 1{,}800$ s) over the total steps for the day t_d.

$$r_f = r_m \cdot \rho_{f(pft)}$$
$$\dot{M}_f = \sum_{t}^{t_d} r_f n_f \Delta t \tag{1}$$

The rate of nitrogen fixed per unit carbon respired, n_f [gN gC^{-1}], follows the functional form by (Houlton et al., 2008). Calibrated constants are taken from (J. Fisher et al., 2010) ($a_{f1} = -6.25$) and (Houlton et al., 2008) ($a_{f2} = -3.62$, $a_{f3} = 0.27$, $a_{f4} = 25.15$) and the soil temperature T_{soil} is prognostic variable of ELM.

$$n_f = a_{f1}\left(e^{a_{f2}+a_{f3}\cdot T_{soil}\left(1-0.5\cdot\frac{T_{soil}}{a_{f4}}\right)} - 2\right) \tag{2}$$

2.2. Plant Acquisition of Aqueous Soil Nutrients

Two of the nutrient competition schemes in ELM are compatible with FATES (CB and RD, see below for details). These schemes are completely separate implementations with different scientific hypotheses. In both, FATES cohorts compete with other cohorts, as well as microbes and mineral surfaces (for phosphorus) for aqueous nutrients in each discrete soil layer j. (The CB scheme does allow for occlusion of ammonium and nitrate in clay soils) Plants compete for (a) ammonium (NH_4) with decomposer and nitrifier microbes, (b) nitrate (NO_3) with decomposer and denitrifer microbes, and (c) phosphate (PO_4) with decomposer microbes and mineral surfaces.

In the native "big-leaf" vegetation representation in ELM, each functional type competes for nutrients as a group. In contrast, FATES enables many cohorts of different sizes and functional types, all to compete independently for resources with soil competitors (typical cohort counts on a site can number anywhere from tens to more than a thousand, depending on local biodiversity and modeler decisions on how to delineate functional groups and size-similarity). Both CB and RD schemes require each cohort to provide a potential uptake rate, or uptake capacity, for each mineral nutrient species ($\hat{M}_{u,NH_4(j)}$, $\hat{M}_{u,NO_3(j)}$, or $\hat{M}_{u,PO_4(j)}$ units [kg m^{-2} s^{-1}]). The actual net daily uptake flux $\dot{M}_{u(s,j)}$ [kg m^{-2} day^{-1}] results from the competition schemes, which we denote with a generic "competition function" $\Gamma_{c(j,t)}$. The Relative Demand (RD) (P. Thornton et al., 2007) method distributes nutrient uptake to competitors in proportion to their demands. Their definition of demand is equivalent to our definition of uptake capacity $\hat{M}_{u,s}$, because we assume the plant demand for nutrient is its capacity for uptake. It also provides controls to scale up or down the relative competitiveness of each entity when total mineralized nutrients are less than total demand. If the total demand exceeds availability, all uptake rates are down-scaled to ensure that the scheme does not generate negative soil N and P concentrations. The Capacity Based (CB) (Zhu et al., 2019) method utilizes a Michaelis-Menten approach to estimate the simultaneous uptake of competing entities with half-saturation parameters, and is therefore influenced by the soil aqueous nutrient concentrations. The exact form of the competition functions are described in Zhu et al. (2019). Both the RD and CB competition models have representations of phosphatase activity following methods of X. Yang et al. (2014) and Wang et al. (2010) respectively.

FATES calculates plant growth and allocation on a daily basis, hence, the total daily uptake for each cohort includes the sum of the uptake over each of the total number of j_s soil layers and sub-daily time-steps (of duration Δt seconds) over the total for the day t_d.

$$\dot{M}_{u(N)} = \sum_{j}^{j_s} \sum_{t}^{t_d} \left(\hat{M}_{u,NH_4(j)} \cdot \Gamma_{c,NH_4(j,t)} + \hat{M}_{u,NO_3(j)} \cdot \Gamma_{c,NO_3(j,t)}\right) \Delta t$$
$$\dot{M}_{u(P)} = \sum_{j}^{j_s} \sum_{t}^{t_d} \left(\hat{M}_{u,PO_4(j)} \cdot \Gamma_{c,PO_4(j,t)}\right) \Delta t \quad (3)$$

The nutrient uptake capacity of a FATES cohort is defined by the per-plant fine-root biomass $C_{(fr)}$ [kg plant^{-1}], the plant density n_p [plants m^{-2}], the fraction of fine-root biomass in each soil layer $f_{fr(j)}$ (see Text S2 in Supporting Information S1), and the maximum uptake rate per unit fine-root biomass $\nu_{\max(\mathrm{pft})}$. This parameter is unique to each mineral nutrient chemical species (NH_4, NO_3, PO_4) for each PFT represented by FATES [kg^{-1} s^{-1}]. Cohort density and fine-root biomass are prognostic variables in FATES.

$$\hat{M}_{u,NH_4(j)} = \nu_{\max,NH_4} \cdot C_{(fr)} \cdot n_p \cdot f_{fr(j)}$$
$$\hat{M}_{u,NO_3(j)} = \nu_{\max,NO_3} \cdot C_{(fr)} \cdot n_p \cdot f_{fr(j)} \quad (4)$$
$$\hat{M}_{u,PO_4(j)} = \nu_{\max,PO_4} \cdot C_{(fr)} \cdot n_p \cdot f_{fr(j)}$$

For the RD approach, the nitrate uptake capacity $\hat{M}_{u,NO_3(j)}$ is handled slightly different than Equation 4. With RD, uptake for nitrogen happens sequentially. The uptake capacity for ammonium and nitrate are combined, and used to drive uptake first from the ammonium pool. This will fulfill some of the plant's needs, and reduce the joint uptake capacity. The remaining joint uptake capacity is then applied to draw down the nitrate pool.

2.3. Losses and Re-Acquisition During Turnover

FATES tracks the daily turnover from senescent tissues on live plants with a carbon loss rate $\dot{C}_{t(o)}$ and nutrient loss rates $\dot{M}_{t(o,s)}$ [kg plant^{-1} day^{-1}] for all non-reproductive plant tissue pools: leaf, fine-root, sapwood, storage, and structural wood, for each cohort. These turnover fluxes are non-episodic, and the rates are controlled by the turnover period parameter $\tau_{(o,\mathrm{pft})}$ [years] associated with the plant's phenological dynamics, which are PFT dependent. The storage, sapwood, and structural wood all share the same turnover rate which is associated with branch-fall. A module that explicitly tracks damage legacies and represents degraded crowns exists (Needham et al., 2022), but is not used here to reduce confounding model factors during analysis.

$$\begin{aligned}\dot{C}_{t(o)} &= C_{(o)}/\left(365\cdot\tau_{(o,pft)}\right)\\ \dot{M}_{t(o,s)} &= M_{(o,s)}/\left(365\cdot\tau_{(o,pft)}\right)\end{aligned} \tag{5}$$

Plants retranslocate a portion of nutrients before leaf and fine-root tissues are shed during senescent turnover. In plain terms, the plants may move nutrients that are bound and or stored in the leaves and fine-roots into other organs of the plant, to avoid loosing these resources when leaves and roots are shed. This rate $\dot{M}_{ra(o,s)}$ [kg plant^{-1} day^{-1}] is drawn from the turnover rate, is directed towards plant storage $M_{(so,s)}$, and is removed from the litter mass flux. There is no retranslocation during fire, and no retranslocation from wood tissues. This retranslocation happens at a constant proportion for leaves $\omega_{lf(s,\mathrm{pft})}$ and fine-roots $\omega_{fr(s,\mathrm{pft})}$ [kg^{-1}] specific to each nutrient (N or P) and PFT. Plants with high retranslocation rates will require less nutrient acquired from other sources, and will generate litter with lower nutrient density per unit carbon. A description of how retranslocation rates are estimated is described in Section 3.1.

$$\begin{aligned}\dot{M}_{ra(lf,s)} &= \dot{M}_{t(lf,s)}\cdot\omega_{lf(s,pft)}\\ \dot{M}_{ra(fr,s)} &= \dot{M}_{t(fr,s)}\cdot\omega_{fr(s,pft)}\end{aligned} \tag{6}$$

Litter mass nutrient fluxes from senescent turnover of live plants follow the same proportion rules and constants as carbon for how they are proportioned into the labile, lignin and cellulose litter pools. For more details, see the FATES technical manual (FATES-Development-Team, 2019).

2.4. Definition of Plant Organ Targets

In FATES-PARTEH, plants grow (to the extent possible, as described below) their organs to preserve observationally constrained allometric relationships. Diameter to height relationships follow Martínez Cano et al. (2019), and diameter + height to biomass follow Chave et al. (2014). As the plant grows and increases in stature (defined by stem diameter at reference height d), these allometric functions define a target carbon mass for each organ, $\grave{C}_{(o)}$. The plant will always attempt to allocate resources such that mass in an organ matches the target (i.e., replace what has been lost), before it attempts to further grow in stature. The method of defining carbon targets in FATES remains unchanged from (R. A. Fisher et al., 2015; C. D. Koven et al., 2020) for all organs except fine-root. Fine-root mass targets now vary as a function of carbon and nutrient storage. This is a key new model mechanism introduced in this work and is explained in Section 2.6. Details on carbon targets and allometry functions for the other organs can be found in the FATES technical manual (FATES-Development-Team, 2019).

Nutrient targets $\grave{M}_{(o,s)}$ for leaf, fine-root, sapwood, and structural wood seek to maintain a constant stoichiometry (i.e., constant P:C and N:C ratios), defined as parameter constants $\alpha_{(o,s,\mathrm{pft})}$ specific to each PFT, element (N or P) and organ.

$$\grave{M}_{(o,s)} = \alpha_{(o,s,pft)}\cdot C_{(o)} \qquad (o = lf, fr, sa, de) \tag{7}$$

Unlike the other organs, the nutrient to carbon ratio of the reproductive tissues and storage ($o = re$, so) are not defined directly by parameter constants. FATES, like many vegetation demography models, does not mechanistically resolve germination or other processes of plants below a minimum recruitment size (Hanbury-Brown et al., 2022); instead it assumes that a fraction of carbon flux allocated to reproduction emerges as new recruits at some time later. We extend this approach to nutrients as well. The stoichiometry of reproductive tissues is set to

match the nutrient to carbon ratios of a newly recruited plant (i.e., a plant with the smallest trackable stem diameter $d = d_{\min}$). This approach means that only the nutrients that are needed to produce recruits with a known stoichiometry are allocated to reproduction, and represents the optimal reproductive allocation stoichiometry that also satisfies mass conservation. FATES initializes newly recruited plants with no reproductive tissues, and they start "on-allometry" (i.e., when their actual mass matches the allometrically defined target).

$$\alpha_{(re,s,pft)} = \frac{\sum \dot{M}_{(o,s)}}{\sum \dot{C}_{(o)}} \qquad (d = d_{\min}, \quad o = lf, fr, sa, de, so) \tag{8}$$

The target nutrient storage $M_{(so,s)}$ is a special case, because it is not associated with a specific tissue. Therefore the target is scaled ($\mu_{(s,\text{pft})}$) based on the target nutrient content of the leaves when "on-allometry." Alternative hypotheses are available for users to test, allowing for storage capacity to scale off of any combination of other organs (e.g., sapwood, fine roots).

$$\dot{M}_{(so,s)} = \mu_{(s,pft)} \cdot \dot{M}_{(lf,s)} \tag{9}$$

2.5. Plant Allocation and Mass Balance Accounting

Both the carbon and nutrient fluxes in the plant and soil systems are mass conservative (i.e., all mass fluxes are accounted for and nothing is created or destroyed). Supplemental nitrogen and phosphorus are often added to the soil in the early years of a spin-up simulation. These effectively 'accelerate' the accumulation of nutrient pools in the soil, and the unresolved processes pf primary succession. These fluxes are tracked in the overall balance as well. The FATES code performs mass-balance checks at both plant and landscape (i.e., contains all disturbance history patches in each FATES site) scale every day. The following rules are stated explicitly for nutrients M, but are also valid for carbon C. The sum of daily allocated nutrient $\dot{M}_{a(o,s)}$ over all organs, should equal the difference between the plant's total gains for the day $\dot{M}_{g(s)}$ and losses due to exudation $\dot{M}_{e(s)}$. The total change in mass over the course of the day $M_{(o,s)}$ is therefore the difference between what is allocated $\dot{M}_{a(o,s)}$ and lost in turnover $\dot{M}_{t(o,s)}$.

$$\begin{aligned} \sum_o \dot{M}_{a(o,s)} &= \dot{M}_{g(s)} - \dot{M}_{e(s)} \\ \dot{M}_{(o,s)} &= \dot{M}_{a(o,s)} - \dot{M}_{t(o,s)} \end{aligned} \tag{10}$$

For nitrogen, the daily gain $\dot{M}_{g(s=N)}$ includes aqueous uptake $\dot{M}_{u(s=N)}$ and symbiotic fixation $\dot{M}_f$. As per the ELM soil biogeochemistry model, any nitrogen made available by free-living fixers in the soil are assumed to be added directly to the aqueous NH_4 pool, and does not need to be explicitly included in this calculation.

$$\begin{aligned} \dot{M}_{g(s=N)} &= \dot{M}_{u(N)} + \dot{M}_f \\ \dot{M}_{g(s=P)} &= \dot{M}_{u(P)} \end{aligned} \tag{11}$$

The model considers three phases for allocation. In each phase, the mass pool for the daily gain $\dot{M}_g$ is reduced as portions of this mass are transferred into plant organs $M_{(o,s)}$. This phase proceeds sequentially in this order, as described next.

- Phase 1: Replacement of Turnover
- Phase 2: Stature Growth
- Phase 3: Remainder and Overflow

2.5.1. Allocation Phase 1: Replacement of Turnover

In the first phase, replacement of tissues lost to turnover is controlled by a prioritization scheme, whereby a user controlled parameter indexed by plant organ $\delta_{(o)}$ is used to assign priority. Organs with the highest priority have a $\delta_{(o)}$ of 1, organs with the lowest priorities will have larger values of $\delta_{(o)}$. A priority of one indicates the organ of interest has the first opportunity, along with other organs with that priority, to replace losses and thus increase the

mass of the organ toward the allometric target (turnover losses shift organ masses "off-allometry"). Other organs with incrementally increasing $\delta_{(o)}$ are then allowed to replace losses while there is still mass in the daily gain pool $\dot{M}_g$. The highest priority organs ($\delta_{(o)} = 1$) have some special considerations to how they are applied (see Text S1 in Supporting Information S1). This flexible scheme reflects persistent uncertainty over the prioritization of allocation by plants and in principle allows rapid hypothesis testing.

The amount of nutrient $\dot{M}_{a(o,s)}$ (or carbon) sent to each organ is driven by the deficit between the actual element mass of the organ and its target mass $\grave{M}_{(s,o)}$. We define a set of organs $\Theta_{1(p)}$ (subscript 1 is for "phase-1" allocation") at priority level p, and the fraction of the total allocation demand that can be filled $f_{a(s)}$ for all organs in this priority level (bounded between 0 and 1). The allocation for each organ is simply its portion of the total replacement demand, scaled by the total replaceable fraction $f_{a(s,p)}$.

$$f_{a(s,p)} = \min\left(1, \dot{M}_{g(s)} \Big/ \sum_{\Theta_{1(p)}} \max\left(0, \grave{M}_{(s,o)} - M_{(s,o)}\right)\right)$$
$$\dot{M}_{a(o,s)} = f_{a(s,p)} \cdot \max\left(0, \grave{M}_{(s,o)} - M_{(s,o)}\right) \Big/ \sum_{\Theta_{1(p)}} \max\left(0, \grave{M}_{(s,o)} - M_{(s,o)}\right) \quad (12)$$

With each successive allocation, mass is removed from the daily gain $\dot{M}_{g(s)}$.

2.5.2. Allocation Phase 2: Stature Growth

If mass remains in all of the daily gain pools ($\dot{M}_{g(s=N)}$, $\dot{M}_{g(s=P)}$, and $\dot{C}_g$) following the replacement phase, the plant will grow in stature. The stem diameter will increase, the target masses of the plant organs (which are tied allometrically to diameter) will increase, and the mass of each organ will increase. All organs grow together as a group, but exceptions can occur for numerical reasons (this is discussed Text S3 in Supporting Information S1). This set of organs that are "on-allometry" are defined as set Θ_2.

The first task is to determine which of the three elements (C, N or P) is in shortest supply and will limit growth. We do this by estimating the mean stoichiometric ratios of the potential new plant growth. Note that to get the relative proportions of new mass allocated to the organs, we evaluate the derivative of the target carbon with respect to change in diameter d, $\frac{d\grave{C}_{(s,o)}}{dd}$, for the organs in set Θ_2, which can be retrieved the from allometric functions at the current stem diameter. The estimated mean stoichiometries (represented by the two summation terms in the brackets to the right of the $M_{g(s)}$ term in Equation 13) are then used to transform the daily nutrient gain into an equivalent carbon $\dot{C}_{g,eq(s)}$ gain.

$$\dot{C}_{g,eq(s)} = \dot{M}_{g(s)} \left[\sum_{\Theta_2} \frac{d\grave{C}_{(o)}}{dd} \Big/ \left(\sum_{\Theta_2} \alpha_{(ft,s,o)} \frac{d\grave{C}_{(o)}}{dd} \right) \right] \quad (13)$$

The minimum of the actual carbon gain $\dot{C}_g$ and the two equivalent carbon gain pools $\dot{C}_{g,eq(s)}$ then defines the carbon that is available for stature growth $\dot{C}_{sg}$.

$$\dot{C}_{sg} = \min\left(\dot{C}_g, \dot{C}_{g,eq(s=N)}, \dot{C}_{g,eq(s=P)}\right) \quad (14)$$

The carbon fluxes into each plant organ are solved via a set of coupled differential equations, conducted via numerical integration from bounds zero to $\dot{C}_{sg}$ for each organ in set Θ_2. The proportion of carbon gain directed to each organ is defined by the derivative of the diameter-to-mass allometry functions, as a fraction of the sum of all derivatives in set Θ_2. The derivatives of the target masses with respect to diameter $\left(\frac{d\grave{C}_{(o)}}{dd}\right)$ are readily available by differentiating the allometry functions. These are coupled equations because they are all simultaneously drawing down $\dot{C}_{sg}$ together, and the derivatives are continuously changing as they grow.

$$\dot{C}_{a(o)} = \dot{C}_{a(o)} + \int_0^{\dot{C}_{sg}} \left[\frac{d\dot{C}_{(o)}}{dd} \Big/ \left(\sum_{\Theta_2} \frac{d\dot{C}_{(o)}}{dd} \right) \right] d\dot{C}_{sg} \tag{15}$$

To handle the allocation of nutrient gains, the same allocation rules from Phase 1 are applied here in Phase 2, using the updated carbon biomass of each organ just explained. Refer to Equations 7 and 12. It should be noted that this modeling hypothesis holds the stoichiometries of plant organs (aside from storage) to the values provided by the parameter constants $\alpha_{(ft,s,o)}$. Small deviations may periodically occur, but they will be corrected automatically by the nature of the algorithm.

2.5.3. Allocation Phase 3: Remainder and Overflow

Daily gain pools ($\dot{M}_{g(s=N)}$, $\dot{M}_{g(s=P)}$, and $\dot{C}_g$) that were not limiting stature growth or replacement may still be available and must be allocated to storage or removed from the plant. Unlike other pools, we allow storage to exceed the target, up to a maximum "overflow" capacity that is based on the target and a user-defined PFT-level parameter constant $\mu_{ov(\mathrm{pft})}$. An overflow flux $\dot{M}_{ov(s)}$ captures this transfer from gains to storage; carbon fluxes follow the same rules as nutrients and are omitted for simplicity.

$$\begin{aligned} \dot{M}_{ov(s)} &= \max\left(0, \min\left(\dot{M}_{(so,s)}\left(1 + \mu_{ov(ft)}\right) - M_{(so,s)}, \dot{M}_{g(s)}\right)\right) \\ \dot{M}_{g(s)} &= \dot{M}_{g(s)} - \dot{M}_{ov(s)} \\ \dot{M}_{a(so,s)} &= \dot{M}_{a(so,s)} + \dot{M}_{ov(s)} \end{aligned} \tag{16}$$

If the storage overflow capacity is full and there are still gains (i.e., $\dot{M}_{g(s=N)} > 0$) that have not been allocated, the plant will exude residual nutrient $\dot{M}_{e(s)}$ into the metabolic (i.e., from labile sources, contains no lignin or cellulose) litter pool with vertical profile fluxes proportional to the fine-root density of each soil layer. If excess carbon remains, there are two options to get rid of the excess $\dot{C}_e$. The default method is to burn it off as autotrophic respiration. Alternatively, users can also opt to exude the carbon with the same partitioning rules along with the nutrients. As will be described in the next section, this model features optimization process that seeks to balance uptake of carbon and nutrients, which will also serve to minimize these excesses. This is evaluated in the analysis.

2.6. Dynamic Fine-Root Biomass Response

Along with symbiotic relationships with nitrogen-fixing bacteria, plants also modify their network of fine-roots to regulate uptake of mineralized nutrient (Forde & Lorenzo, 2001). Some plant and ecosystem models have utilized this behavior for some time (de Kauwe et al., 2014; Thornley, 1995), and a dynamic fine-root optimization scheme is detailed here as well. This scheme seeks to adjust resource allocation above- and below-ground in order for plant growth to be equally limited by carbon, nitrogen and phosphorus (Bloom et al., 1985). If the resource limitations on growth are balanced, the relative amount of carbon in storage (i.e., mass of carbon currently in storage $C_{(so)}$ divided by the target amount of carbon storage $\dot{C}_{(so)}$) will match the relative amount of nutrient in storage (i.e., mass of nutrient currently in storage $M_{(so,s)}$ divided by target amount of nutrient storage $\dot{M}_{(so,s)}$). Given the high complexity of within-plant signaling mechanisms that govern allocation and growth of leaf and root tissues, we do not try to mechanistically represent these processes, and instead aim to tractably represent with as few parameters as possible the net effects of these mechanisms via the optimality-based approach developed here.

We quantify a plant's carbon to nutrient balance with the term f_{cn}, see Equation 17. The term is calculated for the two nutrient elements and takes the maximum, which represents the nutrient with lowest relative storage. A natural log transform is applied for several reasons: (a) the metric becomes centered on zero, where carbon limited plant is less than and a nutrient limited plant is greater than zero, (b) by not being a ratio, it can be

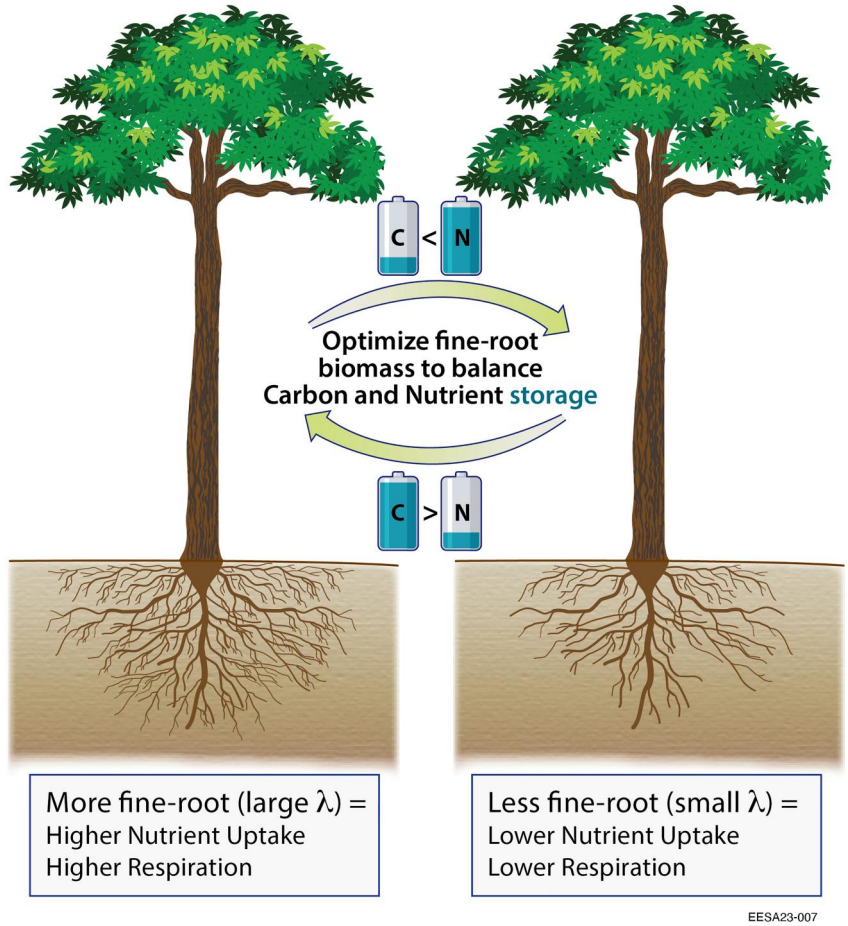

Figure 3. Visualization of the dynamic interaction between differential carbon (C) and nutrient (N) storage and fine-root growth. A plant (left) with proportionally more fine-root will tend to have decreased carbon allocation and increased nutrient allocation, than a plant (right) with proportionally less fine-root. The algorithm presented here seeks to balance these allocations through modifying fine-root growth. *Note that in this diagram, N is representing any nutrient, including nitrogen and phosphorus. Illustration by Diana Swantek, Lawrence Berkeley National Laboratory.

averaged and/or smoothed, and (c) enables additive properties in the algorithm that optimizes fine-root (explained below).

$$f_{cn} = \ln\left(\max_s^{N,P}\left[\frac{C_{(so)}/\dot{C}_{(so)}}{M_{(so,s)}/\dot{M}_{(so,s)}}\right]\right) \tag{17}$$

Fine-root biomass is living tissue that both respires (where maintenance respiration r_m is a function of mass, nitrogen concentration in the tissue, and temperature, following (Ryan, 1991)) and requires continual replacement of losses. An increase in fine-root mass will therefore result in more respiration and lower Carbon use efficiency (CUE) per unit leaf area, but it will also increase capacity for acquiring mineralized nutrients in the soil (recall Equation 4). This is visualized in Figure 3. Thus, positive values of f_{cn} will drive fine-root growth, and negative values of f_{cn} will drive fine-root reductions.

In the FATES allometric model, the fine root target is defined by its proportionality λ with target leaf biomass $\dot{C}_{(lf)}$. The target leaf biomass is defined by the plant's allometry (function of diameter), for details see the FATES technical manual (FATES-Development-Team, 2019).

Table 1
Table Describing the Plant's Response to the f_{cn} *Storage Metric*

Condition		Root response		Plant response
high/positive f_{cn}	→	$\lambda \uparrow$, $C_{(fr)} \uparrow$	→	$r_m \uparrow$, $\dot{M}_u \uparrow$, CUE $\downarrow$
low/negative f_{cn}	→	$\lambda \downarrow$, $C_{(fr)} \downarrow$	→	$r_m \downarrow$, $\dot{M}_u \downarrow$, CUE $\uparrow$

Note. Relatively high and positive f_{cn} drives increases in the fine-root biomass target, which drives increases in fine root biomass, which results in higher respiration (lower carbon use efficiency CUE) yet increased uptake. The reverse is true for low and negative f_{cn} status (i.e., proportionally high nutrient).

$$\dot{C}_{(fr)} = \lambda \cdot \dot{C}_{(l)} \tag{18}$$

In previous versions of FATES, the proportionality λ between leaf and fine-root was a constant user specified parameter. Here, we create an algorithm where it is allowed to be dynamic, and it's value is optimized to result in a differential carbon to nutrient storage f_{cn} that tends towards zero. This system of carbon and nutrient regulation is summarized in Table 1.

In early iterations of developing this hypothesis, we found that a linear model between λ and f_{CN} was prone to over and undershooting an optimal solution, leading to oscillations of λ in steady state climate conditions. To suppress the oscillatory behavior, we included the temporal derivative of f_{CN}. With this, the methodology became a reduced form of a Proportional Integral Derivative (PID) "control-loop" system. In this particular example, f_{cn} is the "process variable" which is driven by a "set-point" (λ). PID controllers also contain an integral term along with the proportion and derivative term. Each of the three terms is given a scaling coefficient, see Equation 19. The calibration of the controller is discussed further in Section 3.3.

$$\lambda_t = \lambda_{t-1} + K_{p(pft)} f_{cn} + K_{i(pft)} \int f_{cn} dt + K_{d(pft)} \frac{\overline{df_{cn}}}{dt} \tag{19}$$

3. Model Calibration and Evaluation

An evaluation of the new model mechanics is performed via simulations at the Smithsonian Tropical Research Institute's Barro Colorado Island (BCI) site in Panama (9° 06′31″ N, 79° 50′37″ W). The site could be described as a semi-deciduous Tropical Rainforest (i.e., dominated by broadleaf evergreens with a mix of deciduous) with a pronounced dry-season (annual rainfall 2.6 [m]). The soils are typical tropical weathered oxisols with a clay texture. The census plot at this site is located on an andesite plateu. The BCI site has an extensive 100 years history of ecological monitoring and analysis in areas including forest demography and census (Condit et al., 2017), growth and mortality (Wright et al., 2010), plant allometry (Cushman et al., 2021; Martínez Cano et al., 2019), nitrogen fixation (Batterman et al., 2013; R. K. Wieder & Wright, 1995), litter and soil biogeochemistry (Mirabello et al., 2013; Powers et al., 2005; Yavitt et al., 2011; Yavitt & Wright, 2001) and more (Muller-Landau & Wright, 2023). It also stands out among tropical monitoring sites for the long (>30 years) and quality controlled meteorological data that is used to drive the FATES model (Faybishenko et al., 2018; Patton, 2019a, 2019b, 2019c, 2019d).

Evaluating the details of both nitrogen and phosphorus dynamics simultaneously would expand the scope beyond what can be covered in one manuscript. We therefore decided to consolidate the evaluation of co-limiting nitrogen and phosphorus simulations to Section 3.5. The remainder of the evaluations focus solely on model response with nitrogen limitations only. Consider that: (a) the model mechanics for phosphorus within the plant are almost exactly the same as with nitrogen with the exception of different parameter constants; (b) nitrogen dynamics modeled in the soil are more complicated than phosphorus because there are two soil mineral pools, a more complicated loss process (i.e., it includes de-nitrification along with leaching) and more dynamic input to the system (i.e., fixation vs. weathering); and (c) there is a separate investigation evaluating phosphorus dynamics at a site in Puerto Rico. The objective here is to determine if the model can capture sensible pattern responses amidst a modest manual parameterization effort that focuses on small sets of parameter perturbations in isolation. The simulation results presented here are not suited as prediction, which would require a parameter calibration exercise using advanced tools to encapsulate a larger set of parameters (including plant carbon dynamics parameters).

Turning off phosphorus limitations is straightforward and achieved by (a) providing a supplementation term that feeds phosphorus directly to soil decomposers, plants, and mineral surfaces so that their nutrient demands are completely met and (b) using a plant uptake affinity parameter $\nu_{\max(s=P)}$ that is excessively efficient (large). This results in the plants ignoring phosphorus effects on the fine-root biomass optimization, acquiring more than enough phosphorus for growth requirements and releasing the excess back to the soil and litter.

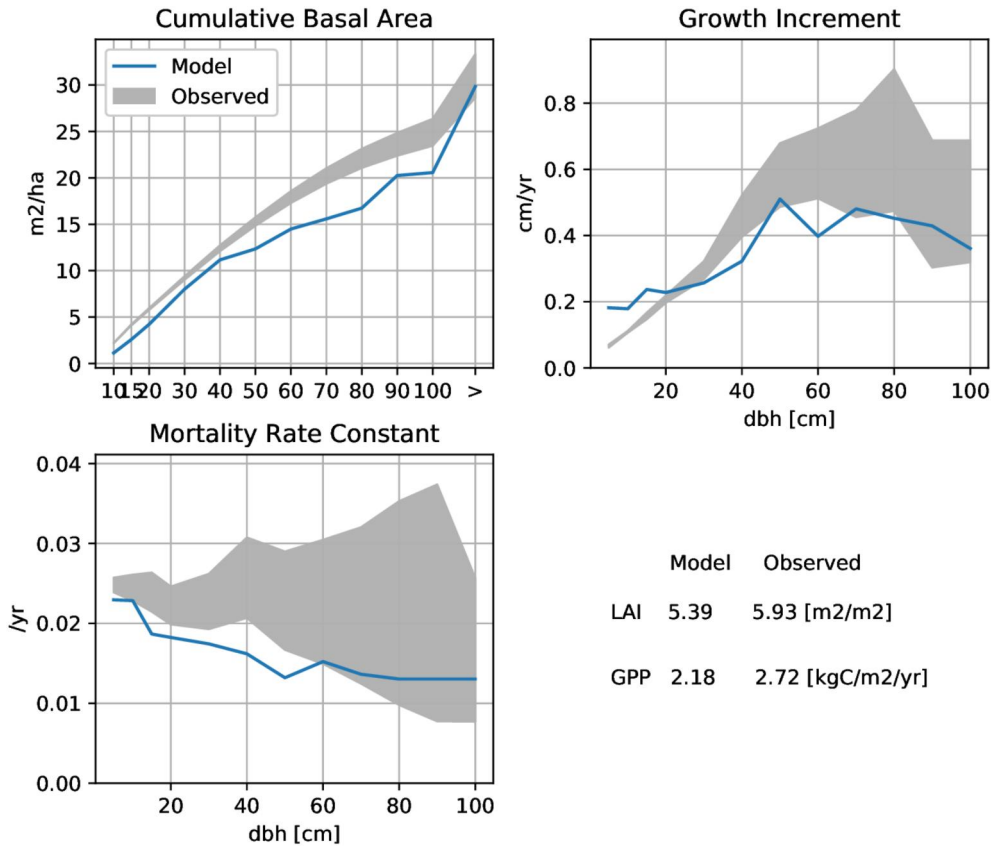

Figure 4. Comparison of observations with the most optimal ELM-FATES parameter set from the ensemble of simulations generated in (C. D. Koven et al., 2020).

3.1. Initial Parameter Calibration

A set of model parameter constants derived from previous research were used as a basis for investigating the sensitivity and function of newly introduced parameters. C. D. Koven et al. (2020) performed a parameter sensitivity analysis of the carbon-only version of ELM-FATES at BCI, where they generated an ensemble of 576 parameter combinations to explore model response to 12 plant traits. We retrieved their model output and compared at different plant size classes to measurements of growth increment (centered at 7.5, 12.5 and 40 cm), mortality rate (centered at 5.5 and 30 cm), and integrated total basal area (<30 cm, <70 cm and all) (Condit et al., 2017). Only two size classes were used for mortality (compared with 3 for basal area and growth increment), to compensate for fewer data points (observations). Scalar values of leaf area and gross primary productivity (GPP) were also compared (Ely et al., 2019). This totals 10 values that can be compared: 10 = 2 size classes of mortality +3 size classes of basal area +3 size classes of growth increment +1 for leaf area and +1 for GPP.

For each ensemble member i and each of these 10 comparison points (subscript j), a difference between the observed and modeled $x_{(i,j)}$ were aggregated to a single fitness metric ϵ_i for each ensemble member, by summing the difference squared between the modeled and observed variables, divided by the variance of the difference across ensembles. The parameter set associated with the simulation that minimized the fitness metric was used as a basis for simulations described here, a comparison of that parameter set with data is provided in Figure 4.

$$\Delta x_{(i,j)} = x_{obs(j)} - x_{(i,j)}$$
$$\epsilon_{(i)} = \sum_j \left(\Delta x_{(i,j)}\right)^2 / \sigma_{\Delta x_{(j)}} \quad (20)$$

Table 2
List of Evaluations That Were Performed

Evaluation group	Description	Competition & nutrients	Period	Section
Calibration				
I	Single cohort simulations for controller sensitivity	RD, N	150 years spin-up	3.3
II	Competition based controller calibration	RD, N	1,000 years spin-up	3.3
		RD, N		
III	Evaluation of base parameterization	RD, N	500 years spin-up + 300 year industrial-era	3.4
		RD, N		
IV	Evaluation of C-N-P model with field data	CB, NP	500 years spin-up + 1,000 year post-spinup	3.5
Sensitivity				
V	Evaluation of competition between symbiotic fixers and non-fixers	RD, N	500 years spin-up	3.6
VI	Evaluation of uptake efficiency ($\nu_{\max(N)}$) and soil N availability	RD, N	500 years spin-up + 300 year industrial-era year industrial-era	3.7
VII	Sensitivity to storage capacity	RD, N	500 years spin-up	SI–S6
VIII	Sensitivity to sub-module hypotheses	RD, N	500 years spin-up	SI–S7
IX	Sensitivity to free-living fixation hypotheses	RD, N	500 years spin-up + 300 year industrial-era	SI–S8

Note. This is partitioned roughly into two-types of objectives, those groups that focus on calibration and evaluation, and those groups that are focused on sensitivity analysis and probing the model. The ELM nutrient competition scheme used (Relative Demand RD or Capacitance Based CB), the nutrients limiting the model, the simulations periods used for each, and the section number are provided. Note that all groups are N limited, and group IV is N and P limited. The last three groups are have been placed in the supplement to keep the manuscript more concise and readable. All simulations were represented by a tropical broadleaf evergreen tree functional type.

Some of the parameters described in Table A1, organ stoichiometries $\alpha_{o,s,\text{pft}}$ and organ turnover rates $\tau_{o,\text{pft}}$, are also derived from the optimization of output (C. D. Koven et al., 2020). For nutrient enabled simulations, there are several new parameter constants that must be estimated. The methods are explained here:

$\omega_{lf(N,\text{pft})}$, $\omega_{lf(P,\text{pft})}$ Leaf nitrogen and phosphorus retranslocation fractions are set at 0.45 and 0.65 respectively, and are derived from measurements of leaf litter and live on-tree leaf stoichiometries at BCNM (unpublished data set provided by S Joseph Wright).

$\omega_{fr(N,\text{pft})}$, $\omega_{fr(P,\text{pft})}$ Evidence of root retranslocation of N and P is sparse, but has been observed in extratropical sites (Freschet et al., 2010; Nambiar, 1987). It is also believed that if roots do not actively retranslocate nutrients before senescent turnover, some portion of nutrient in the newly made root litter will be made available for plant uptake by mycorrhizae. We assume a 0.25 fine-root retranslocation fraction of nitrogen and phosphorus on senescence. Given this uncertainty, this modeling framework could be used in further studies to better understand the sensitivity of different retranslocation assumptions on ecosystem response.

$\delta_{(o)}$ We assign leaves and fine-roots the highest replacement priority, followed by storage and then sapwood and structural wood. We view other prioritization groupings as alternative modeling hypotheses that can be explored in further study.

$\mu_{(N,\text{pft})}$, $\mu_{(P,\text{pft})}$, μ_{ov} The size of the nitrogen storage target $\mu_{(N,\text{pft})}$, and how much storage overflow is allowed μ_{ov} is explored in Evaluation VII (see Table 2 and Text S6 in Supporting Information S1). Understanding plant nutrient storage is a difficult, but there is some thought that plants store enough nutrient for seasonal use (Millard & Grelet, 2010). As a base assumption, for all other simulations, we assume the N and P overflow is 100% of the target, and target storage is 1-times the size of total nutrient bound in leaf tissues.

$\rho_{f(\text{pft})}$ The maintenance respiration surcharge fraction for obligate symbiotic dinitrogen fixation is explored in Evaluation V (See Table 2 and Section 3.6). Symbiotic fixation is turned off in all other evaluations, and total ecosystem fixation is used as a surrogate in those cases.

$\nu_{\max(N)}$ and $\nu_{\max(P)}$ Nitrogen and phosphorus uptake efficiencies were viewed as a model calibration parameters, not readily determined via field measurements. Although calculations based on field inventory,

stoichiometry and turnover data were used to derive a rough starting point. From there, a spectrum of uptake efficiencies were tested for fitness by comparing basal area estimates to field observations (30 m2 ha^{-1}). For RD soil competition mechanics, this resulted in a base value of $\nu_{\max(N)} = 5e^{-9}$ [gN gC^{-1} s^{-1}]. Sensitivity is evaluated in Evaluation VI. The capacitance based competition nutrient scheme has a much smaller actual/potential uptake ratio due to a different algorithm, and thus we arrived at higher values of $\nu_{\max(NH4,NO3)} = 1.75e^{-7}$. Calibration of $\nu_{\max(P)}$ used a similar approach. $= 5e^{-10}$ [gP gC^{-1} s^{-1}] (which was used in Evaluation IV).

$K_{p(\text{pft})}$, $K_{i(\text{pft})}$, $K_{d(\text{pft})}$ The calibration and sensitivity of the PID scaling parameters are covered in Evaluations I and II (see Table 2 and Section 3.3).

3.2. Summary of Evaluations

We conduct a series of evaluations to elucidate the model's behavior. A list of the experiments and the simulations used in each is provided in Table 2. Some simulations are "spin-ups." In these simulations, FATES vegetation is initialized with saplings (if more than 1 plant-functional type is present, the abundances are equal). For the first 30 years of the simulation, nitrogen is added to the soils. Specifically, extra nitrogen is given directly to the plants and microbes if their needs are not met by the existing aqueous nitrogen in the soil (i.e., nitrogen limitations are removed from all competitors). The added N is an artificial model construct that is not intended to represent reality. It is used to give simulations a kick-start (i.e., speed-up) to the spinup by allowing the plant community to develop more quickly and generating a stronger nitrogen fixation flux at the start. After this 30 years phase, nitrogen then accumulates in the system through the natural mechanisms of deposition and fixation (fixation is the dominant input in the system and evaluated further). The modeled decomposition process in this phase uses increased rate constants (often referred to as Accelerated Decomposition (P. E. Thornton & Rosenbloom, 2005)). The atmospheric CO_2 concentration in spin-ups is fixed at pre-industrial levels (290 PPM). Eventually, the nitrogen and carbon content of the soils reaches an equilibrium, as the vegetation evolves towards a mature demographic (quantified by a steady basal area distribution across size and functional types) and the litter fluxes from the vegetation reaches a steady state. In all spin-up simulations, phosphorus is supplemented to the competitors, thus turning off its limitation.

The objective of several spin-up simulations were to provide an initial-condition for industrial-era simulations with transient CO_2 concentrations. In those, we determined that the spin-ups had reached steady-state because the log of the absolute value of Net Biome Productivity had reached very small values (approx 10^{-4} [kgC m^{-2} $year^{-1}$]) (C. Koven et al., 2013).

Industrial-era simulations used normal (un-accelerated) decomposition rate constants, initialized size and age structure of vegetation from preceding spin-up simulations, and likewise initialized organic soil C and N pools using a multiplier of the values passed in from the preceding spin-up simulations. If phosphorus is enabled, the primary, secondary, occluded and organic pools are initialized from the data sets of X. Yang et al. (2013), using a nearest neighbor mapping of the gridded data set to the site at BCI. The phosphorus in the vegetation was initialized from the end of the nitrogen-limited spin-up simulations as well because the plant C:P tissue stoichiometries are fixed from observations. In some experiments where simulations were evaluated into the future, CO_2 concentrations follow from scenario SSP2-4.5.

All simulations utilized the 13-year (2003–2016) meteorological record from Faybishenko et al. (2018) to provide ELM-FATES with rainfall, down-welling solar radiation, down-welling thermal radiation, atmospheric pressure, humidity, wind-speed and surface temperature. The simulations were all much longer than the meteorological record, so the forcing was looped. Most experiments made use of the RD competition scheme, solely because this approach is mathematically and conceptually simpler, which is helpful in probing the complexities of the plant dynamics it is coupled with. In evaluation IV, the N and P limited simulations compared with observations, utilized the capacitance based scheme because it was effective at maintaining aqueous soil nutrient pools under high demand from competitors, as well as to see if its dynamics were sensible and coupled correctly.

3.3. Evaluation I and II: Controller Calibration

The three terms in the PID control system (See Section 2.6 and Equation 19) serve distinctly different functions. The proportion term serves to push the process variable back towards its target value ($f_{cn} = 0$) when there

is a large difference between the current and target value. The derivative term serves to promote stability by suppressing rapid change in the process variable. The integral term is most useful in reducing small and/or persistent biases between the process variable and its target; as the bias grows over time it will exert greater influence to change the set variable. In testing the PID controller and exploring all three terms, we were able to achieve stable results without the integral term, so we decided to set it's scaling constant K_i to zero for this study.

This system of nutrient cycling is fairly complex, with many plant and soil actors competing for and cycling resources, all amongst changing meteorological conditions. The plants are not experiencing a steady availability of nutrients for acquisition, and thus the relationship between controller set point (root proportion λ) and the process variable (storage ratio f_{CN}) are continually experiencing perturbations. To reduce the impact of these perturbations in destabilizing the control system, we apply a multi-day smoother to the derivative term. We use simple exponential smoothing where the future smoothed value X_{t+1} is updated by the instantaneous value Y, the previous smoothed value X_t and a weighting factor D synonymous with the number of time-points (days) over which to weight the instantaneous variable: $X_{t+1} = X_t \cdot (1 - 1/D) + Y \cdot (1/D)$. In the experiments described here, we apply an $D = 10$ days smoother. We also tested 5 and 20 days smoothing windows. Ultimately, reasonable controller response was found with all windows depending on the strength of the scaling constants.

In Evaluation I, special reduced complexity simulations were conducted over a two dimensional log-scale grid search of the K_p and K_d terms from Equation 19. These reduced complexity simulations turned off recruitment and disturbance, which resulted in a simulation of a single plant cohort over a 100 years life-cycle trajectory. Each simulation was assessed for the variance and mean of the process variable $f_{CN(N)}$ (Figure 5), leaf to fine-root biomass multiplier λ (set point, Figure S5.1 in Supporting Information S1) and growth increment (an indicator of optimization of resource use, Figure S5.2 in Supporting Information S1).

The grid search shows that the model simulations are stable and viable (i.e., the plants survive and can adequately adapt their root sizes to become productive) over a large range of parameters (>2 orders of magnitude each). However, no single PID parameter combination has emerged as promoting better model results over the others. Evaluation II seeks to determine this. We create a simulation with four different functional types of plants that compete against each other for resources. A comparison of their basal area trajectories, and the root proportion λ of newly recruited plants in open and exposed sunlight are shown in Figure 6. The plant functional types have the same parameters (i.e., traits) and initial seedling density (this is a spin-up style simulation) with the exception of different PID controller constants. These parameter couplets are labeled a, b, c, and d in Figure 5.

The "C" PID parameter couplet was most effective at rapidly adjusting to the competitive resource environment and homing in on a reasonable λ value fairly quickly, (see the right panel of Figure 6), thus initially occupying the canopy. The "B" and "D" parameter couplets, while not dominating during any phase, persisted through the simulation. The "A" PID parameter couplet eventually out-competes "C" to dominate the canopy. From a theory standpoint, it may be interesting in future work to consider how these PID parameters represent adaptation timescales of different plants, and how those timescales may affect competition. At this point, we focus on a practical perspective, as this exercise has helped to determine a set of PID constants (i.e., "C") that can be used to calibrate and evaluate the rest of the nutrient dynamical model. We acknowledge that these parameters do not affect model outcomes in isolation, and likely have correlation with other parameters that will be investigated in later evaluations. Therefore, parameter set C should not necessarily be viewed as the most optimal, but rather a good candidate to explore the model mechanics further. Other users of the ELM-FATES-CNP model can modify these constants in the parameter file if interested.

3.4. Evaluation III: Towards an Optimality-Based Root Allocation Model

The purpose of this experiment is to view the emergent stand structure of the simulated vegetation under a nitrogen limitation driving the fine-root biomass optimization algorithm. In Figure 7, size-structured estimates of Basal Area, Above Ground Biomass, and the leaf to fine-root proportion term λ partitioned into canopy and under-story plants, are projected across time. All plots show the signature of a spin-up simulation, where over the course of several hundred years the trees grow into the larger size classes from saplings. By the completion of the simulation, there is a fairly uniform distribution of basal area across size classes. There is also a signature of inter-annual variability at any given size. This feature emerges due both the inter-annual variability

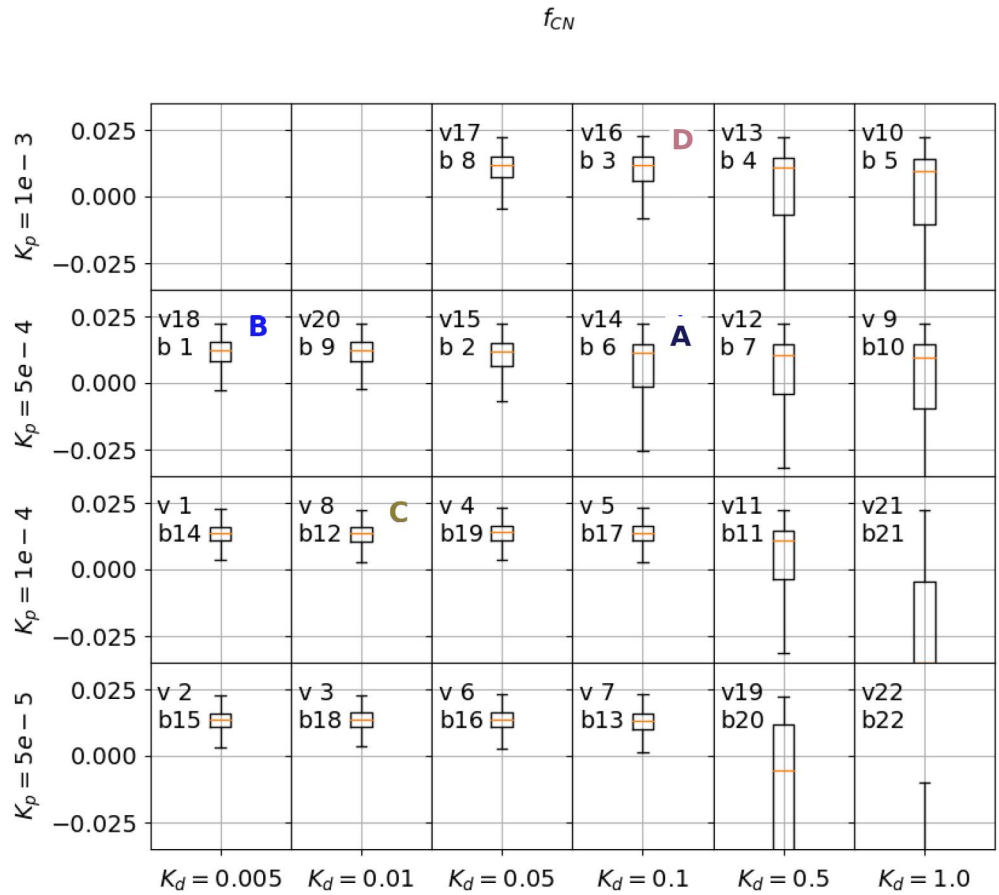

Figure 5. Box plots of the mean (orange line), inter-quartile range (box) and the 2.5 quartile ranges (fliers) for relative storage of carbon to nitrogen variable (and Proportion Integral Derivative controller process variable) $f_{CN(N)}$, over a range of proportion and derivative controller settings. The values next to "v" and "b" indicate the ascending rank of each parameter couplet for bias and variance. Test v1 and b1 had the lowest variance and biases. Couplets designated A, B, C and D are used in the follow-up simulation. The color of the letters is similar to those shown in Figure 6.

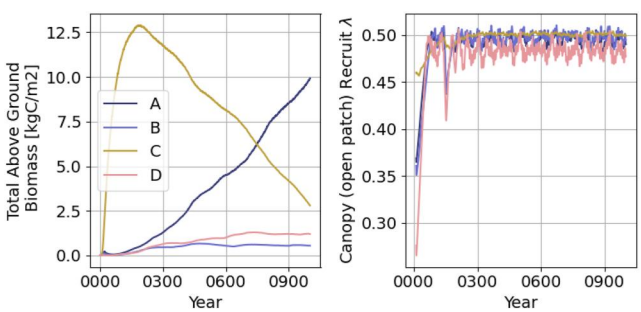

Figure 6. ELM-FATES simulation output containing four competing plant functional types, labeled (a–d). These four PFTs have identical traits and parameters, with the exception of their proportion and derivative proportional integral derivative (PID) parameters. The values of their PID parameters are provided in 5. The right hand panel shows the mean root proportionality λ term for the different PFTs for open patch recruits. Patches that are open, do not have closed canopies and thus light availability to recruits. Recruit λ values are chosen for evaluation here to avoid the confounding affects of size on root proportion.

of the meteorological data set and to the internal dynamics of the cohorts (as similar cohorts fuse together, and grow from one size-classification to a larger one). Other simulations (not shown) were conducted that removed the inter-annual meteorological signal by looping a single year of data, and a similar pattern emerged there as well.

The λ values (i.e., the proportion of fine-root biomass relative to leaf biomass) in the canopy plants are distinctly and consistently larger than those in the understory. This proportion is driven solely by the plant's nitrogen and carbon storage differential, which is a direct result of its relative need for carbon or nitrogen. Therefore plants modeled in the understory have lower fine-root proportions because they need less nitrogen than carbon compared to canopy plants of the same size. All plants (canopy and understory) have access to the same nutrient environment regardless of canopy position, so these differences are driven purely by their ability to capture carbon. Canopy plants have greater access to light and have increased primary productivity compared to their understory neighbors. This increased productivity places a greater demand on nitrogen acquisition to keep pace with more rapid construction of plant tissues. Moreover, the increased productivity of the canopy plants provides adequate carbon

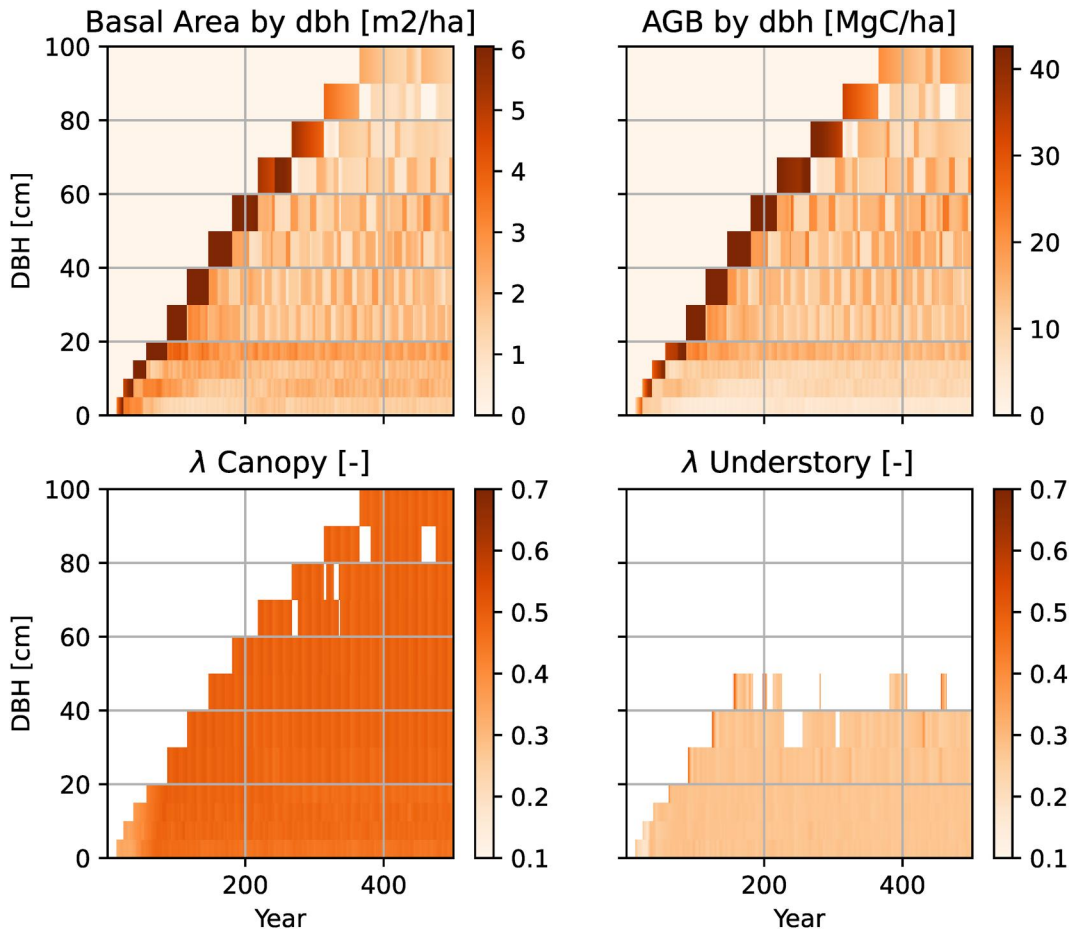

Figure 7. Evaluation of the size structure of vegetated biomass accumulation, and the size and canopy position structure of the fine-root proportion term λ [gC fine-root gC−1 leaf]. Canopy plants display distinctly larger λ values than understory plants at similar size classes.

reserves to pay for the increased respiration associated with more fine-root biomass. Plants that are in the understory have limited access to light and subsequently lower productivity. Without the carbon to build new tissues there is a correspondingly lower demand on nutrients to match the construction costs of the carbon. This potentially triggers a response in the plant to decrease investments (respiration costs of fine-roots) in the acquisition of nutrients it doesn't need. A very similar simulation (which was testing a higher vcmax parameter 50 vs. 30.5), is presented in Figure S10.1 in Supporting Information S1. That simulation was more "top heavy" in its representation of vegetation biomass, that is, distinctly more in the largest size classes and was quicker to reach those sizes. It also demonstrates that while the understory plants can reduce their fine-root biomass, they do not achieve the same CUE of the canopy plants, which is also indicative of their lower, almost stagnant, growth rates.

We note here a qualitative agreement between this emergent behavior in ELM-FATES-CNP, of plants in a higher light environment shifting their allometry towards greater allocation to roots, with observations similarly showing that plant allometric plasticity across light gradients favors a greater root biomass fraction under higher light levels (Poorter et al., 2012).

3.5. Evaluation IV: Comparison of N and P Co-Limited Simulations With Field Observations

This section demonstrates the co-limiting affects of simulating both nitrogen and phosphorus together. Comparisons are then made with observations at the BCI site. Observations of fine-root biomass and mineralized

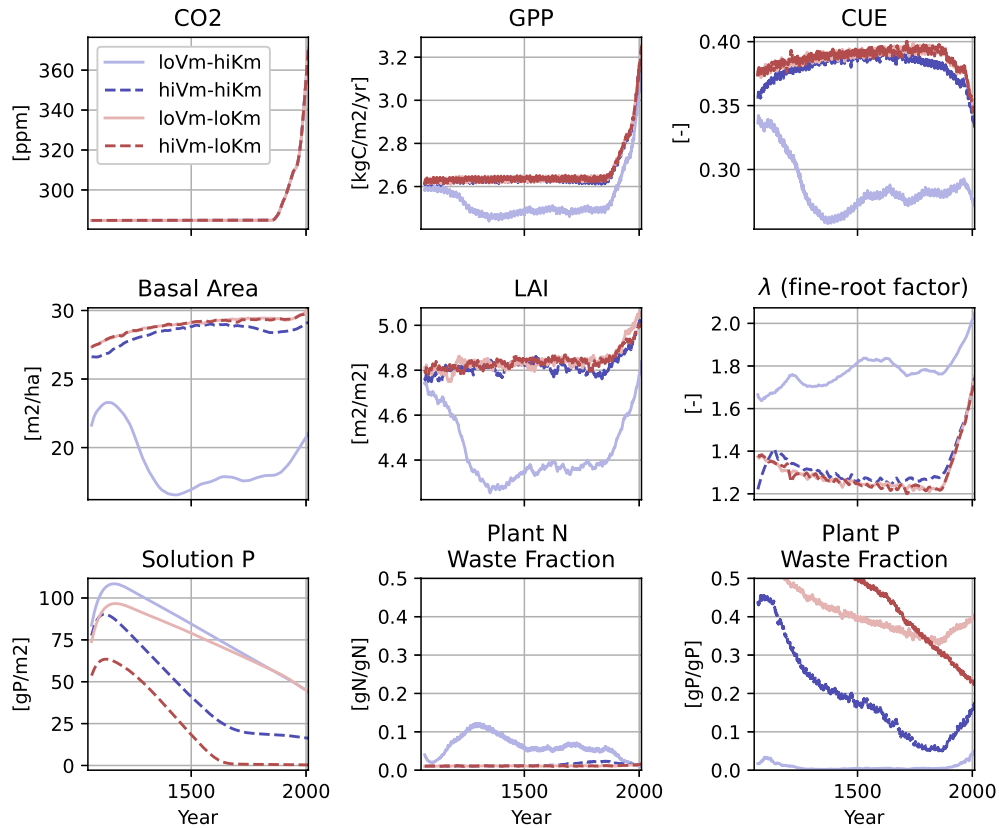

Figure 8. Time series results from four simulations limited by Nitrogen and Phosphorus. The four simulations present perturbations (a lower value and a higher value) of the two major plant phosphorus Michaelis–Menten uptake controls, maximum uptake $\nu_{\max(P)}$ and Michaelis constant $K_{m(P)}$. Low $\nu_{\max(P)} = 2e^{-10}$, high $\nu_{\max(P)} = 5e^{-10}$, low $K_{m(P)} = 0.01$, high $K_{m(P)} = 0.5$. Nutrient waste fractions are calculated as the amount of nutrient effluxed from the plant divided by the plant's total uptake.

nutrient content was made available via the FRED3 database (Iversen et al., 2017). Each of these simulations utilizes the same initial condition, which is the final state of a pre-industrial nitrogen-only spin-up simulation.

These C, N and P limited simulations provided an opportunity to study and probe key parameters related to plant P uptake. Here we focus on the two Michaelis-Menten parameters in the Capacitance Based (CB) nutrient competition scheme (Zhu et al., 2019), the maximum uptake capacity $\nu_{\max(P)}$ and the Michaelis constant $K_{m(P)}$. The Michaelis constant inversely impacts the competition function Γ_c (see Equation 3) along with aqueous soil phosphate concentration $[P]$:

$$\Gamma_c \propto 1/\left(K_{m(P)} + [P]\right) \tag{21}$$

This was the first FATES evaluation to simultaneously compare above-ground (LAI and Basal Area) and below-ground (fine-root biomass profiles) model output to observations (including previous carbon-only experiments). It was evident that with the base calibrations of parameters that directly regulate CUE, productivity was not in balance with the turnover and respiration losses that came with more fine-root biomass. To address this, two parameters that directly impact CUE were updated. The catalytic capacity of Rubisco, $V_{c,\,\max}$, was increased from 30.9 (a legacy value used in previous FATES-ELM runs (C. D. Koven et al., 2020), and other evaluations in this study) to a value of 71 ((Lamour et al., 2023) and personal communication), and the fine-root turnover time-scale $\tau_{(fr)}$ was increased from 1 to 3 years.

Similar to calibrations with N (described in other sections), P uptake parameters were searched manually. A time-series of four simulations that demonstrate the coordinated effects of using relatively high and low $\nu_{\max(P)}$ and $K_{m(P)}$ are shown in Figure 8.

Table 3
Integrated Relative Bias Scores for Carbon and Nutrient Targets in the CNP Simulation ($\nu_{max(P)} = 5e^{-10}$, $K_{m(P)} = 0.01$), Arranged in Acending Order for Basal-Area (BA), LAI, Fine-Root Biomass (FR), and Mineralized Nutrient Concentrations of Ammonium (NH4), Phosphate (PO4) and Nitrate (NO3)

B_{BA}	B_{LAI}	B_{FR}	B_{NH4}	B_{PO4}	B_{NO3}
−0.0393	−0.107	−0.949	−1.45	1.52	−1.99

Note. These scores are a companion to the differences presented in Figures 9 and 10.

With overly high $\nu_{max(P)}$ values, the plants acquire more phosphate than needed, dumping what they could not use into the labile organic litter pool. This is quantified by the waste fraction (see lower right panels of Figure 8), the ratio of effluxed nutrient relative to the uptake through the roots. When evaluated together, this tells us which nutrient (N or P) is in shortest supply to the plant (lower waste fraction). Simulations with very high values of $\nu_{max(P)}$ (not shown) would ultimately run into issues with availability because P was being pulled out of aqueous phosphate and sequestered in soil/litter organics. Alternatively, plants with overly low values of $\nu_{max(P)}$ could not acquire enough phosphate to meet their needs and stagnated due to their inability to meet construction costs. With low values of the Michaelis constant $K_{m(P)}$ (increased competitiveness), the plants preferentially acquire phosphate at the expense of decomposers and mineral surfaces. Depending on the strength of $\nu_{max(P)}$ and the Michaelis constants of the decomposers and the mineral surfaces, the plant community would potentially survive. But in the best scenarios the canopy persisted amidst unrealisticaly low concentrations of soil phosphate, and in the worst scenarios (not shown) the canopy would collapse because the decomposition cycle would slow to a halt thereby essentially stopping the production of phosphate. Increasing the plant $K_{m(P)}$ (decreased competitiveness) promoted an increased equilibrium level of aqueous phosphate, correspondingly promoting more plant uptake even at low $\nu_{max(P)}$. The values of $\nu_{max(P)}$ and $K_{m(P)}$ in Figure 8 are somewhere in the middle of the endpoints described.

The simulation in Figure 8 using the lower $\nu_{max(P)}$ and the higher $K_{m(P)}$ constant (i.e., less competitive) showed less P wastage than the other three. Moreover, both N and P waste fractions dominated at different times, displaying co-limitation in the same simulation.

The simulation that maximized competitiveness, that is, $\nu_{max(P)} = 5e^{-10}$, $K_{m(P)} = 0.01$, showed better agreement with results, and is referenced in Table 3, Figures 9, 10, and S9.1 in Supporting Information S1. The fitness of the simulation was primarily based on comparable forest demographics (i.e., basal area, LAI and fine-root biomass), and secondarily with comparable mineralized soil nutrient concentrations (since the primary, secondary, occluded pools are driven externally).

Model predicted fine-root biomass was compared to observed profiles by Yavitt et al. (2011), Yavitt and Wright (2001) and Powers et al. (2005) at BCNM (Figure 9). The model estimated mean concentrations of mineralized nutrients (NH_4, NO_3 and PO_4) (Figure 10) in solution are compared to measurements by Yavitt and

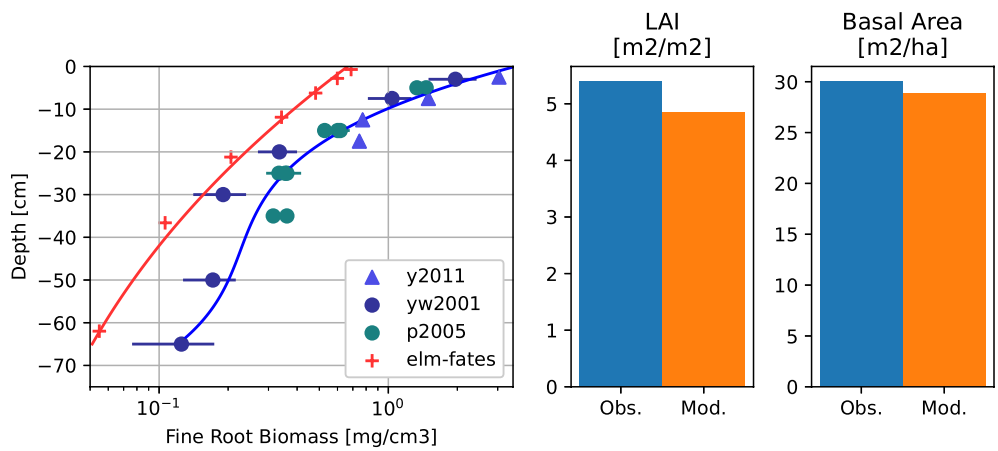

Figure 9. Comparison of ELM-FATES predicted fine-root biomass against observations at BCNM by Yavitt et al. (2011) (y2011), Yavitt and Wright (2001) (yw2001) and Powers et al. (2005) (p2005). All data was filtered to report only estimates of live roots from 0 to 2 mm diameter. Studies that did not differentiate between live and dead roots were corrected using the necromass to livemass ratio of 0.0806 (Yavitt & Wright, 2001). Data points with circles represent measurements on Barro Colorado Island, data points with triangles are on the other side of the river on the Gigante Peninsula. The polynomial fits to the data (used in bias calculations) are shown along with the estimates. Comparisons of basal area and LAI are from Condit et al. (2017).

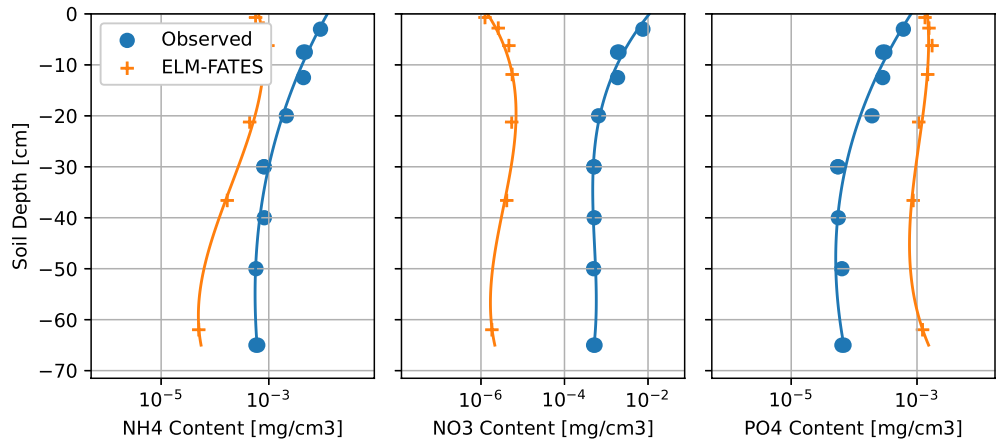

Figure 10. Comparison of ELM-FATES predicted mineralized nutrient concentrations against those observed by Yavitt and Wright (2001). The polynomial fits to the data (used in bias calculations) are shown along with the estimates.

Wright (2001). In this parameterization, the model underestimated fine-root biomass, under-estimated the mineralized N concentrations, and over-estimated the mineralized P concentrations. The low N concentrations is fairly consistent with other simulations in this manuscript. Mineralized N concentrations using the RD soil competition scheme were typically lower compared to the CB scheme. Phosphate concentrations that are lower and more consistent with observations were not overly difficult to achieve in isolation of other verification targets (i.e., ignoring biomass), and were typical of increasing plant and decomposer competitiveness (small value of $K_{m\ (P)}$) and/or increasing phosphate leaching losses from runoff.

Comparisons for fine-root biomass and mineralized nutrient content were made over depth. To generate a comparable statistic, both model and observed quantities were fit with 3rd order polynomials, and then integrated over depth. The integrated quantities for observed x_{obs} and modeled x_{mod} were then compared as a bias statistic B, where $B = 2\ (x_{\text{mod}} - x_{\text{obs}})/(x_{\text{mod}} + x_{\text{obs}})$. This is equivalent to an unsigned relative root mean squared difference statistic on a single data pair. The data fitting was necessary because model and observations where not on the same depth grid, and more than one study contributed to fine-root biomass estimates.

In summary, the CNP module was fairly successful in representing its primary target of basal area and LAI, yet biases on the order of the amplitudes are evident for estimates of fine-root biomass and mineralized nutrients. We discuss potential causes of the observed differences, and the interplay between productivity, nutrient uptake efficiency and total nutrient availability in the discussion.

3.6. Evaluation V: Incorporating Cohort-Scale Symbiotic Fixers

Here we evaluate if the symbiotic nitrogen fixation module can generate an expected ecosystem response. One way to test this is to see if a nitrogen-fixing PFT can coexist with a non-fixing functional type in simulation. In this experiment, the two plant functional types have the same traits with the exception of the symbiotic fixing parameters themselves. This test is a simple proof of concept, and ignores the multifaceted trait space that fixers and non-fixers may occupy.

By introducing symbiotic fixation to the simulation, the pre-existing total ecosystem fixation scheme (Cleveland et al., 1999) must be modified to only represent free-living fixation. This approach is similar to the approach used by CLM5 (Lawrence et al., 2020), which identifies that the original total ecosystem fixation rates estimated in Cleveland et al. (1999) projected low and high ranges of fixation. Here, we downscale the NPP-derived total ecosystem nitrogen fixation rate by a multiplicative scaling factor of 0.2.

For plants to achieve co-existence in this model configuration, the unit cost of symbiotic fixation must be higher than the uptake of aqueous nitrogen at its potential rate (i.e., uptake when aqueous nitrogen is abundant and no source side limitation exists), yet must be lower than aqueous uptake under some amount of limitation. Otherwise, symbiotic fixers would always be more efficient and out-compete non-fixers, not only when nitrogen from the mineralized soil pool is limited. Menge et al. (2022) has made this type of argument, pointing out that the

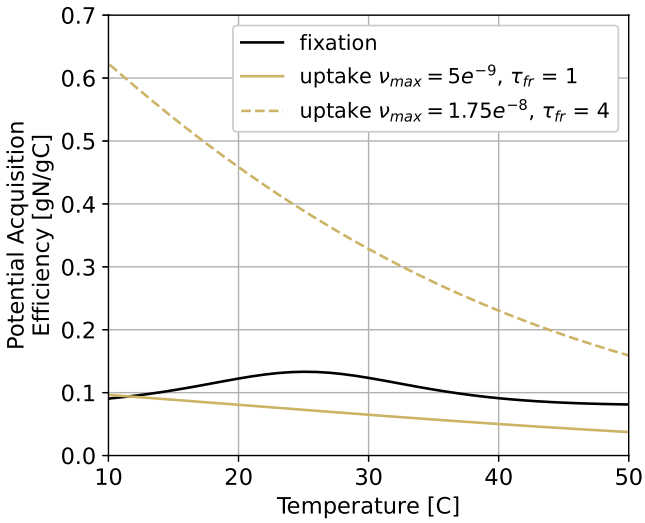

Figure 11. Comparison of the unit carbon efficiency for obligate symbiotic fixation (J. Fisher et al., 2010; Houlton et al., 2008) versus potential aqueous nitrogen uptake under the base parameterization and one with increased efficiency. Carbon costs for uptake efficiency consider maintenance respiration and replacement carbon costs, but not the initial investment.

energetic costs of breaking the triple bonds in N_2 and supporting the nodules in symbiotic fixers are thought to be costly. The expectation is that the two functional types will reach an equilibrium in their relative proportion, where the symbiotic fixers will support a mineralized nitrogen pool to an amount where the carbon costs of actual plant nitrogen uptake balance with that of fixation.

One way to assess the unit carbon efficiency [gN gC^{-1}] (inverse of cost) for potential mineralized nutrient acquisition, is the sum of the potential uptake rate of the plant $\nu_{max(NH4,pft)} + \nu_{max(NO3,pft)}$ [gN gC^{-1} s^{-1}] (for RD based competition), divided by the maintenance respiration and replacement costs of the roots [gC^{-1} s^{-1}]. Note this is the steady state rate, and ignores the initial cost to grow the root. The unit cost of fixation is directly quantified by Equation 2, (J. Fisher et al., 2010; Houlton et al., 2008). In the base parameterization, the carbon efficiency for potential mineralized uptake was lower than the fixation efficiency. We found that by increasing the total potential uptake rate $\nu_{max(NO3)} + \nu_{max(NH4)}$ and increasing the fine-root lifespan $\tau_{(fr)}$ from 1 to 4 years, the potential mineralized uptake efficiency exceeded that of fixation, see Figure 11.

The result of the test simulation is shown in Figure 12. The symbiotic-fixing PFTs were set to apply a 10% surcharge on fine-root maintenance respiration to fuel symbiotic fixation. This experiment also reduced the external N supplementation period from 30 to 5 years, to ensure that the symbiotic fixers had more control over system N supply (Figure 13).

Fixers and non-fixers do show coexistence as demonstrated by their total above-ground biomass. The fixers have lower fine-root biomass fractions λ, which indicates their decreased need for mineralized nitrate and ammonium. Very early in the simulation, the non-fixers are more efficient due to the plentiful mineralized soil nitrogen. But after the supplementation period, plant mineralized nitrogen uptake becomes more limited (see bottom right panel), which then creates a competitive opportunity for the fixer PFT to emerge.

As a whole (considering both PFTs), symbiotic fixation accounted for about 5%–10% of total plant acquisition, and slightly more than 50% of the total nitrogen fixed by the ecosystem (including free-living). The latter is roughly close to what is expected, Batterman et al. (2013) suggested that symbiotic fixation was the dominant mode of introducing nitrogen to the site at BCNM, but within the same order of magnitude. The proportion in the simulation could be increased by further regulating uptake efficiency parameters or scaling down the free-living fixation rate. There are also different symbiotic fixation temperature response functions available (Bytnerowicz et al., 2022), and future ELM-FATES-CNPtesting may use these.

It takes about 500 years in this simulation for the fixer and non-fixer types to reach an equilibrium. Yet, the results are an average of the whole landscape, and not a representation of how a single plot of land recovers from a disturbance. Batterman et al. (2013) estimated that symbiotic fixation peaked near the first decade following a disturbance, but after several decades total fixation flux dwindled considerably. This suggested that symbiotic fixers play an important role in developing the nutrient environment in newly disturbed lands, but perhaps they became less competitive as the nitrogen built up in the soil and vegetation over time. The ELM-FATES-CNP model does have the ability to simulate disturbance and discretely track land of different ages (called "patches") and the plants that inhabit them. However in the current version of the model, the soil column and its biogeochemistry (i.e., nitrogen and phosphorus concentrations in all forms) are the same across patches of all ages, as the patch structure only represents heterogeneity in the aboveground environment. In future versions of the model it would be interesting to see if the competitive dynamic of symbiotic fixers and non-fixers can be achieved over the time-scales of decades where each patch has a dedicated nutrient environment in the soil.

3.7. Evaluation VI: Sensitivity to Parameter Constants That Control Nutrient Availability and Affinity

Evaluation VI tests model response to the intersection of three forces: nitrogen availability, plant nitrogen use efficiency and increasing atmospheric CO_2 concentration. Nitrogen use efficiency is modified by perturbing the

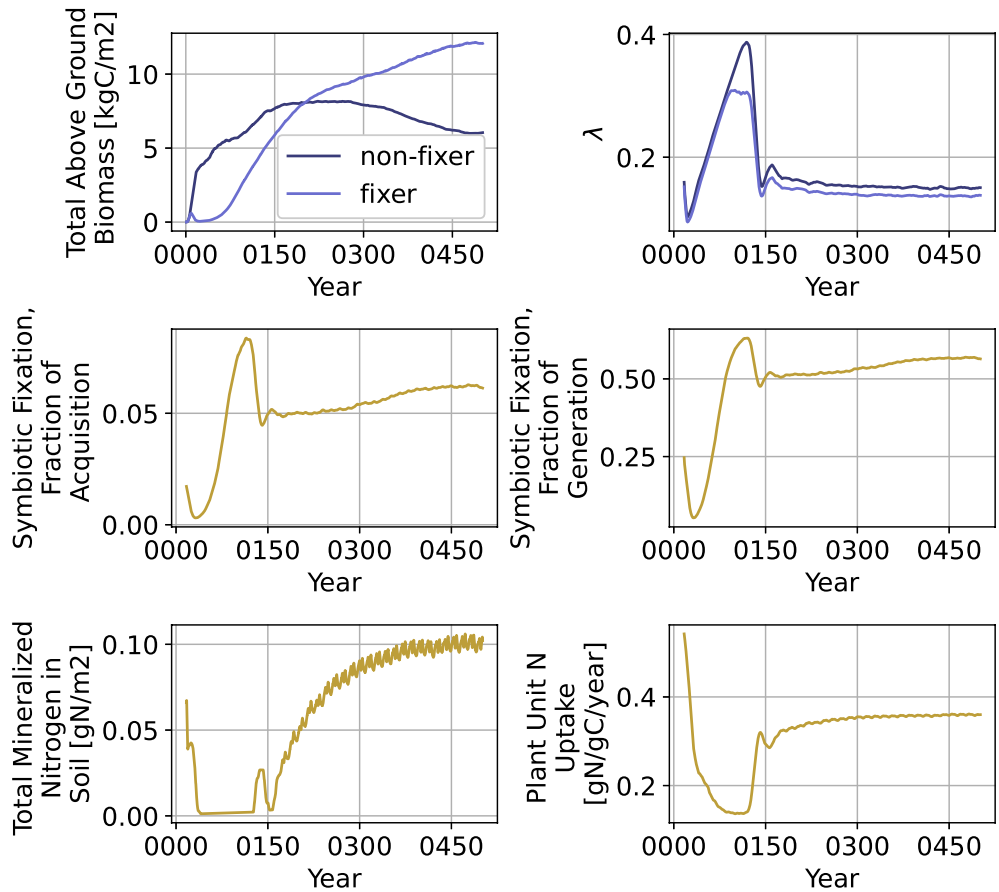

Figure 12. ELM-FATES-CNP simulation with coexistence between a fixer and non-fixer plant functional type. The symbiotic fraction of acquisition, refers to the fraction of plant acquisition that is from symbiotic-fixation, along with mineralized nutrient uptake. The fraction of generation looks at the relative contribution of symbiotic fixation to total nitrogen fixed by the system, also considering free-living fixation.

plant functional parameter constant: unit potential nitrogen uptake rate per mass of fine root (efficiency) $\nu_{\max(\mathrm{pft},N)}$ [gN gC^{-1}]. High values of $\nu_{\max(\mathrm{pft},N)}$ (highly efficient) will acquire more nitrogen for less fine-root carbon. Nitrogen availability is controlled by applying a constant multiplicative scaling coefficient β to the NPP-based total ecosystem fixation function. The β parameter is not listed in Table A1, and is not considered a component of this model because existing total ecosystem fixation schemes were used in this manuscript and the scaling coefficient is only used here to test sensitivity. The four parameter combinations are provided in Table 4, and a time-series of model output that use these four parameter sets are provided in Figure 13.

In all four simulations, there are several patterns that offer straightforward explanations. Increased productivity associated with higher CO_2 concentrations drive higher basal area (biomass) and leaf area, as well as increased demand on nitrogen acquisition to meet greater organ construction costs. Mineralized (aqueous) nitrogen depletes over time, as the new additions to the system (fixation) can not keep pace with the increased uptake. Faced with a greater need for (higher production) and a reduced supply of aqueous nitrogen, the plants respond by increasing uptake capacity by building more fine-roots (λ). With decreased aqueous nitrogen and higher root mass, the unit uptake of nitrogen per unit biomass decreases. The increase in CUE experienced by the plants is diminished (and mostly reversed) when the mineralized nitrogen pools fully deplete, and the plants are forced to respire newly assimilated carbon that cannot be used to build tissues.

Some patterns in the response are explainable, but less straightforward. Mineralized nitrogen depleted first in the low availability simulations, and also slightly earlier in the high versus low affinity simulations. This suggested that plants can be overly competitive for nitrogen, ultimately to their detriment. In simulations with higher uptake affinity, the plants out-competed decomposers, which prevented the decomposers from mineralizing nitrogen into

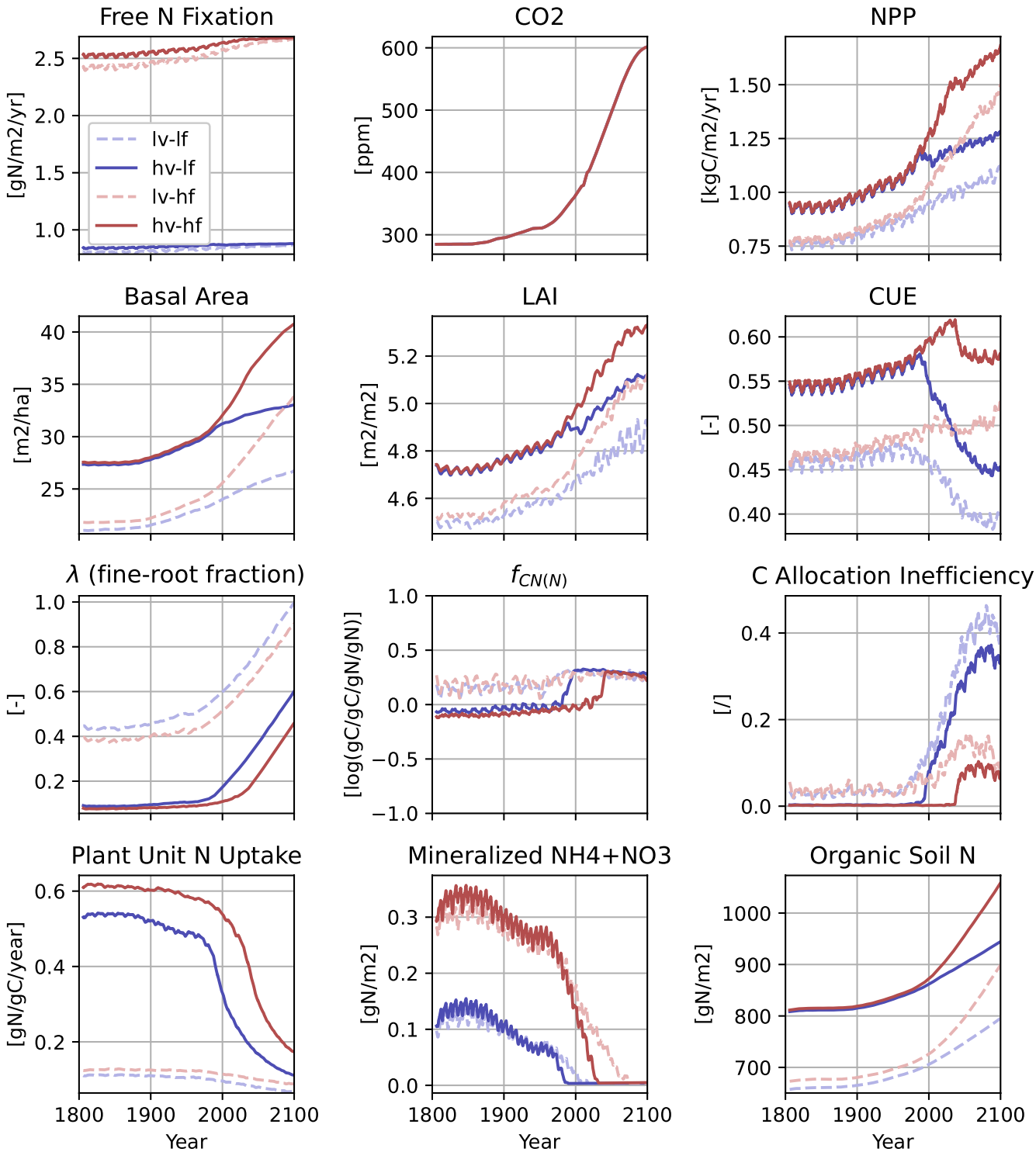

Figure 13. Time series model output for the four simulations described in Experiment VI. Line colors match simulations described in Table 4, where: "lv-lf" is low-affinity low-fixation, "hv-lf" is high-affinity low-fixation, "lv-hf" is low-affinity high-fixation and "hv-hf" is high-affinity high-fixation. The CO_2 forcing signal uses observed industrial-era concentrations and follows the SSP2-4.5 scenario prediction to 2100. With no symbiotic fixation, Free N Fixation is synonymous with total fixation and is the primary source of nitrogen input. Carbon use efficiency is the ratio of net primary production over gross primary production, where NPP accounts (i.e., subtracts) for any extra respiration of "excess carbon," that which couldn't be allocated due to nitrogen limitations. This extra respiration is also captured by "C Allocation Inefficiency," the fraction of grams of excess carbon burned per grams NPP. Plant Unit N Uptake refers to the grams of nitrogen uptake per gram of fine-root carbon.

Table 4
Parameter Combinations for the Four Simulations in Evaluation VI

	Low plant uptake affinity	High plant uptake affinity
low fixation	$\nu_{\max(N)} = 5e^{-9}, \beta = 0.5$	$\nu_{\max(N)} = 2.5e^{-8}, \beta = 0.5$
high fixation	$\nu_{\max(N)} = 5e^{-9}, \beta = 2.0$	$\nu_{\max(N)} = 2.5e^{-8}, \beta = 2.0$

Note. Each simulations used perturbations to only nitrogen acquisition efficiency $\nu_{\max(\mathrm{pft},N)}$ and a scaling coefficient on total ecosystem fixation β. The red (compared to blue) indicates a higher nitrogen availability in the system. The darker shade (compared to lighter) indicates a higher plant uptake efficiency.

the system, which leads to a slightly earlier collapse. It must be emphasized here, that mineralized nitrogen concentrations of zero are not observed at this site. These simulations are intended to stress-test the model to evaluate its behavior under end-member type parameter calibration environments. However, recall from Evaluation IV that perturbations of the Michaelis-Menten competition parameters K_M for phosphorus displayed that equilibrium values of mineralized nutrient could be calibrated with the Capacitance Based (CB) competition scheme. A discussion on model calibration and generating parameterization that are useful for prediction is provided in the discussion.

Another interesting pattern was the shift in the process variable $f_{\mathrm{CN}(N)}$, from unbiased (i.e. closer to 0) to a bias indicative of a perpetually nutrient limited state. In the high affinity case, the algorithm attempts to rectify the bias by increasing the λ value, however the slowly dwindling supply of aqueous nitrogen continually counteracts the affect that increased fine-root fraction (set variable) should have on the process variable. This raises the question: what is the appropriate time-scale of response for investing in plant nutrient uptake? In these simulations, the PID constants that control λ were chosen for competitiveness in a constant CO_2 environment, but perhaps a parameterization that favors more rapid adaptability would be more competitive in a changing CO_2 environment.

4. Discussion

4.1. Regulation of Nutrient Uptake

There are multiple avenues plants employ to regulate nutrient acquisition, which include the fine-root growth response and obligate symbiotic fixation described in this manuscript. Yet the uptake of nutrient by plants harbors complexity, including modification of not just fine-root biomass, but morphology and structure (e.g., Taylor et al., 2014), the dynamic regulation of ion-specific transport systems within and across the root-soil interface (Crawford & Glass, 1998), considerations of advection and diffusion (e.g., McMurtrie & Näsholm, 2018), symplastic and apoplastic transport (Steudle & Peterson, 1998), enzyme kinetics, symbiotic relationships with facultative nitrogen fixers, algal nitrogen fixation on leaves, mycorrhizal associations and moreover acquisition of other nutrients not considered here (K, Ca Mg, etc).

Employing dynamic fine-root response to nutrient gradients has both an established history in observation (Forde & Lorenzo, 2001) as well as model development (de Kauwe et al., 2014; Farrior et al., 2013; Thornley, 1995). This method differs from the Thornley models in how fine-root growth is controlled, where they tracked the substrate (C and N) concentrations in the roots and shoots dynamically. Several models also down-regulate mineral nutrient uptake in a more facultative form, outside of signaling increases or decreases in fine-root biomass (Kou-Giesbrecht et al., 2021; Thornley, 1995; Thum et al., 2019; Zhu et al., 2019). Thornley (1995) called this downregulation product inhibition, and based it on N concentrations in the roots. Kou-Giesbrecht et al. (2021) identified it as nitrogen stress, and tied it to the deficit of actual to target non-structural nitrogen content in the plant. Thum et al. (2019) downregulates uptake based on "internal-demand" which also assesses the labile (non-structural) nutrient content in the plant against the nutrient content of roots and leaves. ELM-FATES-CNP does not include this facultative downregulation, for two reasons. The first is that it was not clear how to represent this economically by associating a cost to this regulation. Secondly, an imperative was placed on minimizing the accumulation of parameters with the interest of using nutrient limitations in global simulations and their calibrations. We do however acknowledge this as a limitation of the model. In particular, ammonium, nitrate and phosphate uptake are all tied to the same optimization target, fine-root biomass response, and cannot up and down-regulate independent of each other. While it is unclear how to quantify both the timescale and the costs of regulated transport systems in the fine-roots, particularly using a tractable set of parameter constants calibrated for a global set of plant functional types, regulated transport systems exist (Crawford & Glass, 1998).

Looking towards future model testing and developments, uptake capacity could be associated with dynamic activity levels of the fine roots, as well as the amount of fine-root biomass or their surface area. While many of these processes about to be mentioned are implicitly captured in the work presented here, through maximum uptake capacity of roots and the Michaelis Menten half-saturation constants, their explicit representation could be illuminating. For instance, dynamic activity could be described as enzymatic activity rates, which are tied to nutrient content, the production of exudates to prime decomposition (via mycorrhizae for instance) or to chelate nutrients.

Or, as recently stated, dynamically regulated transport systems for each chemical species could be introduced. This activity could be controlled explicitly by resource investments from the plant (e.g., respiration, carbon and nutrient allocations) and constrained (albeit not explicitly governed or proportional to) by fine-root surface area. Root nutrient uptake could be made more realistic by considering the diffusion and mass transport of nutrients in the soil, root surface area and root architecture using the model of McMurtrie and Näsholm (2018).

4.2. Fine-Roots at the Nexus of Productivity, Resource Availability and Acquisition Efficiency

Potential nutrient uptake (or similarly, plant nutrient demand) in ELM-FATES-CNP is dictated by the amount of fine-root biomass and the maximum uptake rate parameter family ν_{max}, recall Equation 4. As demonstrated in Evaluation IV and VI, small (inefficient) values of ν_{max} drive larger fine-root proportions (λ), and large (efficient) values of ν_{max} drive smaller fine-root proportions λ. The response of λ was also impacted by total system nutrient availability (tested in Evaluation VI by scaling total N addition to the system via community N fixation), and how carbon productive the plants are (See pertubation to catalytic capacity of Rubisco $v_{c,\,max}$ in Evaluation IV). This model has shown an interplay between the processes of how carbon productive and efficient plants are and how nutrient productive and efficient plants are.

In theory we could continue to decrease the uptake efficiency parameter ν_{max} until we achieve more comparable estimates of fine-root biomass. This can not be done in isolation, as to support more fine-root biomass with a similar stand-structure, the plants would need greater productivity and would require a holistic calibration exercise that also looks at net carbon productivity parameters, such as those controlling organ turnover rates, respiration rates and GPP.

However, we take the comparison of fine-root biomass with field data (see Figure 9) with a grain of salt. There is a difference between how the FATES model differentiates a fine-root from other tissues, and how fine-roots are differentiated in the field. FATES has a functional definition, and differentiates fine-roots as tissues that respire at a higher rate than coarse root or below-ground sapwood. Also FATES makes no differentiation of absorbing versus transporting fine-root tissues, or how those tissues respire, turnover or impact nutrient cycling (McCormack et al., 2015).

Also, fine roots in FATES-CNP are treated as absorbing tissues for the purposes of nutrient uptake. At the same time, the model applies a single fine-root lifetime for the purposes of calculating the costs and benefits of fine root allocation. Alternatively, fine-roots are typically differentiated in the field by size (diameter) and order (Iversen et al., 2017), and efforts to reconcile fine root biomass and ^{14}C isotopic ratios have demonstrated two distinct populations of fine roots with widely varying turnover times (Ahrens et al., 2014; Gaudinski et al., 2010). In this respect, there is somewhat of a disconnect between the meaning of fine-root represented in the model and how fine-roots are currently conceptualized to influence plant and ecosystem function. Making a more closely aligned comparison between what the model defines as fine-root, or what sub-classifications it has, and what is measured in the field, would be useful for verification and calibration. Measurements of nitrogen content in fine-roots, either connected to the profiles of carbon biomass via ratios, or as a stand-alone profile would aid in making a cleaner comparison between model and observation. The current model formulation uses total fine-root nitrogen as the basis for the carbon costs of respiration (Ryan, 1991). In future work, we intend to represent different fine root functional populations, their nitrogen content, and associated turnover times to better represent the joint constraints of nutrient uptake rates, root biomass profiles, and root ^{14}C isotopic ratios.

4.3. Looking Ahead to Calibration

The model calibrations performed thus far were driven primarily to achieve fitness in the vegetation structure. However, we also compared against new axes that we had not previously investigated (or calibrated) with the carbon-only model, including fine-root biomass, eddy flux (See Text SI 9.1 in Supporting Information S1) and mineralized nutrient concentrations. On one hand it was encouraging that with nutrient limitations, the model could continue to estimate similar vegetation structure (basal area and LAI) that it had in the carbon-only model. However, there were clear biases between the other model estimated metrics and observations (See Table 3).

In Evaluations IV and VI, we learned that mineralized nutrient uptake capacity (i.e., ν_{max}) would promote increased fine-root proportions in the model, yet this would also drive down total biomass as CUE decreased due to increased respiration and turnover costs. Utilizing newly available estimates of $V_{c,\,max}$ (Lamour et al., 2023),

and updates to decrease root turnover, partially (but not completely) increased the productivity and efficiency of the plant to facilitate the higher fine-root content seen in the root census data. The Eddy flux data (Detto, 2022) (Figure SI 9.1 in Supporting Information S1) suggests there possibly an overly large respiration component, yet it is not clear if that is do to soil respiration over that period, and/or underestimated GPP.

We also learned that the perturbations that focused on model sensitivity to phosphate uptake showed us that modification of uptake capacity $\nu_{\max(P)}$ and the Michaelis constant $K_{m(P)}$ did provide powerful levers to generate different levels of nutrient uptake, and also straight-forward and somewhat differential controls on phosphate availability and plant uptake. No sensitivity of ammonium or nitrate affinity, such as $\nu_{\max(NH4,NO3)}$ or $K_{m(NH4,NO3)}$ were performed against the measured values, and thus compared poorly (See Figure 10). The nitrogen system is also more complex, in that there are two mineralized pools (NH_4 and NO_3 compared to PO_3), a more dynamic gain term (fixation), and another loss term (denitrification) compared to just leaching with phosphate. In a future calibration effort, it is clear that at least one set of nutrient affinites (those for P or those for N) should be calibrated along with the parameters that goven plant carbon balance, and parameters that govern soil nutrient losses and gains (leaching, denitrification, fixation, etc). Moreover, calibrating plant uptake parameters (such as $\nu_{\max(P)}$) are sensitive to the magnitude of the phosphate concentration in solution, which is just as slow to equilibriate as other soil nutrient pool, and may require simulations of 100s of years to generate realizations in a calibration exercise.

In summary, it became clear that a calibration that operates on a broader parameter set of parameters that controls plant carbon balance as well as nutrient uptake affinity and cost is the logical next step. Assuming our representation of modeled and observed fine-root biomass can be rectified, these observations would form a key component of future calibration exercises. Such an exercise would also require more sophisticated toolsets to explore the parameter optimization space (such as Offline Land Model Testbed (Lu et al., 2018; Sinha et al., 2023), the Predictive ECosystem ANalyzer (LeBauer et al., 2013), LAVENDAR (Pinnington et al., 2020), etc.)

4.4. Other Limitations and Future Work

This research focused on a single evaluation site, and did not explore the model hypotheses in extra-tropical ecosystems, or the competition dynamics between plants with different functional traits. Part of this decision was based on practicality. Developing a model comparison test-bed requires high-fidelity meteorological drivers and soils data. This study also utilized a calibration of the carbon-only version of the model (per the BCI site's specific demographics) to form a solid foundation for the perturbations and analyses of the new nutrient relevant parameters and module switches. While the type of data used is available at other sites, it requires pre-processing, conversion and site-specific adaptation. Moreover, the scope of this manuscript was already quite large. As explained elsewhere, this constrains the study to a demonstration of the model's capacity to test its hypotheses and make sensible and reasonable responses to stimuli, and no intention has been made in making predictions. Future extensions to this work could evaluate model response to environmental gradients in soil conditions or climate forcing, and in those cases it would pertinent to perform calibration exercises across multiple sites, tropically or extra-tropically. Further studies could also investigate biodiversity and interaction among plants (of different functional types) that may differ in how aggressive or conservative their nutrient acquisition strategies may be, or how tradeoffs related to these strategies may or may not lead to coexistence.

The model hypothesis presented here represents plant organ stoichiometries that are time-invariant traits associated with the plant's functional type. While there is evidence for leaf nutrients and photosynethic parameters such as $V_{c,\,\max}$ to covary, and it is hypothesized to be important (Walker et al., 2014), the mechanistic understanding of how leaf nutrient stoichiometry varies in time, and how it affects $V_{c,\,\max}$, are not well understood. In the current configuration, effects of tight versus loose correlation between these $V_{c,\,\max}$ and leaf nutrient content, on productivity and competitive outcomes could be explored through Perturbed Parameter Ensembles in future work. Our FATES development has provided a software infrastructure to facilitate these types of developments, and the open-source code and our paper encourages these types of analyses for future work.

This model formulation has not explicitly incorporated mycorrhizal activity or its affects on nutrient availability. In a sense, the effects of mycorrhizae are implicit or subsumed in the soil decomposition and nutrient competition schemes. However, without explicitly representing mycorrhizae, it is impossible to capture the symbiotic benefits of the association with the plants alone, and not just the broader affects of releasing mineralized nutrient to the soil system. It would be interesting to incorporate and test hypotheses of explicit mycorrhizal interactions, and their

effects on nutrient cycling. The ELM-FUN model explicitly represents mycorrhizal interactions and could potentially help in this endeavor.

Calibration and uncertainty in Earth System Simulators has become an ever increasing challenge as all facets of the models steadily become more complex, with more tune-able parameter constants and greater process uncertainty. It was imperative that this formulation struck a balance between the desire to represent numerous complex processes and the desire to have a stable model that uses a reasonably small number of parameter constants (particularly those that cannot be directly retrieved from measurements). Without these concessions, terrestrial biosphere models cannot be extended beyond a handful of measurement-rich testbed sites.

5. Conclusions

This paper presents a framework that allows combining forest demography modeling with nutrient cycling, with a goal towards balancing increased physical process representation while limiting to the extent possible new parameters and associated complexity. In their own right, the limitations of nutrients to plant growth, and the ability to represent plant demographic controls on growth, mortality and disturbance, are both vitally important to representing the flow of global carbon stocks in a changing world. This work introduces the necessary step of combining these two major concepts. Land-surface models are starting to combine higher levels of complexity in these major demographic and nutrient feature components, in both land models (ED2-MEND-NCOM (Medvigy et al., 2019)), as well as fully coupled ESMs (LM4.1-BNF (Kou-Giesbrecht et al., 2021; Sulman et al., 2019)), for use in better exploring quantifying and understanding how these dynamics interact with global change, and this work demonstrates a model foundation to further such efforts.

The series of experiments presented here has demonstrated that this model framework can generate sensible patterns of ecosystem response, using a modest parameter constant calibration effort. To summarize: (a) a small grid search of PID constants K_d and K_p rendered values that enable the model to adapt stable fine-root biomasses with reasonable levels of nutrient and/or carbon efficiency losses, (b) perturbations to parameters that control nutrient storage μ, μ_{ov} did not exert undue model instability or variability, and (c) subtle differences in how the model culls unnecesary roots and removes unused carbon showed modest differences in model output. The number of newly introduced and salient (to nutrient cycling) model parameters that aren't readily derived from field meausurements (i.e., stoichiometry α, and leaf retranslocation ω_{lf}) that exerted strong control on model response is small (namely, the uptake affinity parameters $\nu_{\max}$ and K_m). Balancing model complexity with model robustness and preventing over-calibration is of critical importance and has been identified as a key need in land-surface modeling endeavors (Prentice et al., 2015).

The new model hypothesis captures a few simple yet important concepts. Nutrient acquisition requires resources and that the construction of plant biomass is limited by the acquisition of nutrients. In this case, the payment is the maintenance respiration, construction and turnover replacement cost of the fine-roots. The current model hypotheses can also work with existing hypotheses in free-living and symbiotic nutrient fixation. Finally, the dynamicism of fine-root proportion allows for a new competitive niche, where understory plants have a new method to conserve resources when there is low access to light and productivity.

Appendix A: Table of Variables and Parameters

This appendix contains a table of variables and parameter constants that are used throughout the manuscript and its supplemental material.

Table A1
Non Exhaustive List of Variables and Parameter Constants in the Functionally Assembled Terrestrial Ecosystem Simulator (FATES) Nutrient Cycling Model

Symbol	Description	Units
State variables		
$C_{(o)}$	Carbon mass	[kg]
$\grave{C}_{(o)}$	Target carbon mass	[kg]
$M_{(o,s)}$	Nutrient mass	[kg]

Table A1
Continued

Symbol	Description	Units
$\grave{M}_{(o,s)}$	Target nutrient mass	[kg]
d	Reference stem diameter	[cm]
λ	Leaf to fine-root target biomass multiplier	[–]
f_{cn}	The relative storage of carbon over the relative	
	Storage of nutrient, for the maximum (more limited) of nitrogen and phosphorus	[–]
External and diagnostic variables		
f_{trim}	Canopy trim fraction	[–]
n_p	The number of plants in a cohort per square meter	[plants m^{-2}]
$f_{fr(j)}$	The fraction of fine-root biomass in each soil layer	[kg^{-1}]
Fluxes		
$\hat{M}_{u,NH4(j)}$	Plant ammonium uptake capacity in each soil layer	[kg m^{-2} s^{-1}]
$\hat{M}_{u,NO3(j)}$	Plant nitrate uptake capacity in each soil layer	[kg m^{-2} s^{-1}]
$\hat{M}_{u,POx(j)}$	Plant phosphate uptake capacity in each soil layer	[kg m^{-2} s^{-1}]
$\dot{M}_{u(s)}$	Daily uptake of mineralized soil nutrients in solution	[kg day^{-1}]
$\dot{C}_g$	Daily carbon gain	[kg day^{-1}]
$\dot{M}_{g(s)}$	Daily nutrient gain	[kg day^{-1}]
$\dot{M}_f$	Daily nitrogen gained through symbiotic fixation	[kg day^{-1}]
$\dot{M}_{e(s)}$	Excess nutrient exuded back to soil	[kg day^{-1}]
$\dot{C}_{t(o)}$	Daily carbon lost to turnover	[kg day^{-1}]
$\dot{M}_{t(o,s)}$	Daily nutrient lost via turnover	[kg day^{-1}]
$\dot{M}_{a(o,s)}$	Daily nutrient net allocated	[kg day^{-1}]
$\dot{r}_e$	Excess respiration of unusable carbon	[kg day^{-1}]
$\dot{r}_f$	Respiration cost to fix Nitrogen	[kg day^{-1}]
Parameter constants		
$\alpha_{(o,s)}$	Nutrient stoichiometric target for	
	Non-labile tissue, nutrient mass per carbon mass	[kg^{-1}]
$\tau_{(o,\text{pft})}$	Non-mortal turnover timescale of plant organs	[years]
$\omega_{lf(s,\text{pft})}$	* Leaf retranslocation fraction of nutrient on turnover	[kg^{-1}]
$\omega_{fr(s,\text{pft})}$	* Fine-root retranslocation fraction of nutrient on turnover	[kg^{-1}]
$\mu_{(s,\text{pft})}$	* Proportion of target nutrient stored	
	Per target nutrient in tissues	[kg^{-1}]
μ_{ov}	* Fractional overflow of storage (all chemical species)	
	The plant will hold before exuding or respiring	[–]
$\rho_{f(\text{pft})}$	* Maintenance respiration surcharge fraction for obligate symbiotic dinitrogen fixation	[–]
$\nu_{\max(s)}$	* Maximum nutrient uptake demand per fine-root biomass	[kg^{-1} s^{-1}]
$\delta_{(o)}$	* Allocation priority	[index]
$K_{p(\text{pft})}$	* Proportion term scaling parameter in PID controller	[–]
$K_{i(\text{pft})}$	* Integral term scaling parameter in PID controller	[–]
$K_{d(\text{pft})}$	* Derivative term scaling parameter in PID controller	[–]

Note. All Mass and Mass Fluxes Are Assumed to be "per Plant" [$plant^{-1}$]. External Variables Refers to Those Variables That Are Resolved by FATES Processes Outside the Scope of This Manuscript and Are Described in the FATES Technical Manual. Parameter Constants Denoted With * Are Newly Introduced in This Study. Proportional Integral Derivative Stands for Proportion Integral Derivative, and Is the Controller Used to Search for Optimal Fine-Root Biomass

Appendix B: Software Features

The processes described here are encoded in a modular and extensible software structure. It is modular because the software for the plant algorithms do not reference data structures from the FATES (or other) model and uses a lightweight coupler to communicate with FATES. This approach allows the plant model to be ported to any terrestrial biosphere model that uses a cohort or individual plant type of scaling approach. It is extensible because the software is written so that other configurations of plant organs (e.g., leaf spatial layering, storage pools with different functions, mycorrhizae, etc.) and chemical elements (e.g., Potassium, Magnesium, etc.) can be readily adapted, if the user can provide relevant parameter constants and the surrounding terrestrial biosphere model can accommodate the boundary fluxes. Further, the FATES model code that processes litter fluxes has been written to loop over the self-describing data structures for the chemical elements present (instead of explicitly defining new variable primitives for each mass pool or flux associated with a chemical species).

Data Availability Statement

The data and software code used to reproduce the model simulations and analysis in this manuscript have been made publicly available. The "Next Generation Ecosystem Experiment–Tropics" project provides model driver data at the Barro Colorado Island Site, including soils and meteorological data (Knox et al., 2019). The data can be found here: https://ngt-data.lbl.gov/dois/NGT0086/. Both the FATES and E3SM models use Git (https://git-scm.com/) version control to manage their software, and Github (https://github.com/) to host their software. The model software of both projects and their dependencies are publicly available. Readers who wish to either reproduce or do similar work in this manuscript are encouraged to install git and use it to clone the E3SM model, also Zenodo DOIs are provided. FATES will be imported as a submodule of E3SM. To initialize submodules following a clone, and assuming the user has "checked out" the correct tag or branch, they should run the command "git submodule update –init –recursive".

The specific E3SM tag used in this research is DOI 10.5281/zenodo.7684977, 10.5281/zenodo.7684977; or the github tag can be found here: https://github.com/rgknox/E3SM/releases/tag/elm-fates-cnp-ms (Edwards et al., 2023).

The specific FATES tag used in this research is DOI 10.5281/zenodo.7685350, 10.5281/zenodo.7685350; or the github tag can be found here: https://github.com/rgknox/fates/releases/tag/fates-cnp-ms-anlsys (FATES-Development-Team, 2023).

The python analysis scripts (contained in (FATES-Development-Team, 2023)) used to generate the figures in this manuscript are provided in the directory: "./ms-analysis/".

This file (contained in (FATES-Development-Team, 2023)) will patch the default FATES parameter file to generate parameterizations specifically for one tropical evergreen PFT at Barro Colorado Island Panama: https://github.com/rgknox/fates/blob/fates-cnp-ms/parameter_files/patch_default_bciopt224.xml.

A nix-type "shell" script (contained in (FATES-Development-Team, 2023)) is provided, that was used to build and setup the simulations. This script should be executed from the directory: "./cime/scripts." This file also assumes that the driver data package listed above is unpacked in the same directory as well. The user will need to modify many of the paths in the script to accommodate their file structure. This script should facilitate other users running simulations at BCI, but this file is provided as-is, and absolutely no support will be provided for making this script work. https://github.com/rgknox/fates/blob/fates-cnp-ms/parameter_files/create_bci_fatescnp_mscopy.sh.

Acknowledgments
This research was supported as part of the Next Generation Ecosystem Experiments-Tropics, funded by the U.S. Department of Energy, Office of Science, Office of Biological and Environmental Research. RF acknowledges funding by the European Union's Horizon 2020 (H2020) research and innovation program under Grant Agreement No. 101003536 (ESM2025—Earth System Models for the Future) and 821003 (4C, Climate-Carbon Interactions in the Coming Century). Steve Paton of the Smithsonian Tropical Research Institute was involved in providing the original measurements of meteorological data used to drive these simulations. The Smithsonian Tropical Research Institute was the provider of the original unprocessed meteorological data, as well as the provider of the census data as referenced in (Condit et al., 2017), see http://biogeodb.stri.si.edu/physical_monitoring/research/barrocolorado. Helene Muller-Landau provided consultation on the interpretation of raw census data that was used in the calibration of the carbon-only model.

References

Ahrens, B., Hansson, K., Solly, E. F., & Schrumpf, M. (2014). Reconcilable differences: A joint calibration of fine-root turnover times with radiocarbon and minirhizotrons. *New Phytologist*, *204*(4), 932–942. https://doi.org/10.1111/nph.12979

Allen, K., Fisher, J. B., Phillips, R. P., Powers, J. S., & Brzostek, E. R. (2020). Modeling the carbon cost of plant nitrogen and phosphorus uptake across temperate and tropical forests. *Frontiers in Forests and Global Change*, *3*. https://doi.org/10.3389/ffgc.2020.00043

Arora, V. K., Katavouta, A., Williams, R. G., Jones, C. D., Brovkin, V., Friedlingstein, P., et al. (2020). Carbon–concentration and carbon–climate feedbacks in CMIP6 models and their comparison to CMIP5 models. *Biogeosciences*, *17*(16), 4173–4222. https://doi.org/10.5194/bg-17-4173-2020

Batterman, S., Hedin, L., van Breugel, M., Ransijn, J., Craven, D., & Hall, J. S. (2013). Key role of symbiotic dinitrogen fixation in tropical forest secondary succession. *Nature*, *502*, 224–229. https://doi.org/10.1038/nature12525

Bloom, A. J., Chapin, F. S., III, & Mooney, H. A. (1985). Resource limitation in plants-an economic analogy. *Annual Review of Ecology and Systematics*, *16*(1), 363–392. https://doi.org/10.1146/annurev.es.16.110185.002051

Bonan, G., Williams, M., Fisher, R., & Oleson, K. (2014). Modeling stomatal conductance in the earth system: Linking leaf water-use efficiency and water transport along the soil–plant–atmosphere continuum. *Geoscientific Model Development*, *7*(5), 2193–2222. https://doi.org/10.5194/gmd-7-2193-2014

Bonan, G. B., Oleson, K. W., Fisher, R. A., Lasslop, G., & Reichstein, M. (2012). Reconciling leaf physiological traits and canopy flux data: Use of the TRY and FLUXNET databases in the Community Land Model version 4. *Journal of Geophysical Research*, *117*(G2). https://doi.org/10.1029/2011jg001913

Botta, A., Viovy, N., Ciais, P., Friedlingstein, P., & Monfray, P. (2000). A global prognostic scheme of leaf onset using satellite data. *Global Change Biology*, *6*(7), 709–725. https://doi.org/10.1046/j.1365-2486.2000.00362.x

Braghiere, R. K., Fisher, J. B., Allen, K., Brzostek, E., Shi, M., Yang, X., et al. (2022). Modeling global carbon costs of plant nitrogen and phosphorus acquisition. *Journal of Advances in Modeling Earth Systems*, *14*(8), e2022MS003204. https://doi.org/10.1029/2022MS003204

Brzostek, E. R., Fisher, J. B., & Phillips, R. P. (2014). Modeling the carbon cost of plant nitrogen acquisition: Mycorrhizal trade-offs and multipath resistance uptake improve predictions of retranslocation. *Journal of Geophysical Research: Biogeosciences*, *119*(8), 1684–1697. https://doi.org/10.1002/2014jg002660

Buotte, P. C., Koven, C. D., Xu, C., Shuman, J. K., Goulden, M. L., Levis, S., et al. (2021). Capturing functional strategies and compositional dynamics in vegetation demographic models. *Biogeosciences*, *18*(14), 4473–4490. https://doi.org/10.5194/bg-18-4473-2021

Burrows, S. M., Maltrud, M., Yang, X., Zhu, Q., Jeffery, N., Shi, X., et al. (2020). The DOE E3SM v1.1 biogeochemistry configuration: Description and simulated ecosystem-climate responses to historical changes in forcing. *Journal of Advances in Modeling Earth Systems*, *12*(9), e2019MS001766. https://doi.org/10.1029/2019MS001766

Bytnerowicz, T., Akana, P., Griffin, K., & Menge, D. (2022). Temperature sensitivity of woody nitrogen fixation across species and growing temperatures. *Nature Plants*, *8*(3), 209–216. https://doi.org/10.1038/s41477-021-01090-x

Caldwell, P. M., Mametjanov, A., Tang, Q., Van Roekel, L. P., Golaz, J.-C., Lin, W., et al. (2019). The DOE E3SM coupled model version 1: Description and results at high resolution. *Journal of Advances in Modeling Earth Systems*, *11*(12), 4095–4146. https://doi.org/10.1029/2019MS001870

Chave, J., Réjou-Méchain, M., Búrquez, A., Chidumayo, E., Colgan, M. S., Delitti, W. B., et al. (2014). Improved allometric models to estimate the aboveground biomass of tropical trees. *Global Change Biology*, *20*(10), 3177–3190. https://doi.org/10.1111/gcb.12629

Christoffersen, B. O., Restrepo-Coupe, N., Arain, M. A., Baker, I. T., Cestaro, B. P., Ciais, P., et al. (2014). Mechanisms of water supply and vegetation demand govern the seasonality and magnitude of evapotranspiration in Amazonia and Cerrado. *Agricultural and Forest Meteorology*, *191*, 33–50. https://doi.org/10.1016/j.agrformet.2014.02.008

Cleveland, C., Townsend, A., Schimel, D., Fisher, H., Howarth, R., Hedin, L., et al. (1999). Global patterns of terrestrial biological nitrogen (N_2) fixation in natural ecosystems. *Global Biogeochemical Cycles*, *13*(2), 623–645. https://doi.org/10.1029/1999GB900014

Collatz, G., Ball, J., Grivet, C., & Berry, J. A. (1991). Physiological and environmental regulation of stomatal conductance, photosynthesis and transpiration: A model that includes a laminar boundary layer. *Agricultural and Forest Meteorology*, *54*(2), 107–136. https://doi.org/10.1016/0168-1923(91)90002-8

Condit, R., Pérez, R., Lao, S., Aguilar, S., & Hubbell, S. P. (2017). Demographic trends and climate over 35 years in the Barro Colorado 50 ha plot. *Forest Ecosystems*, *4*(17), 17. https://doi.org/10.1186/s40663-017-0103-1

Crawford, N., & Glass, D. (1998). Molecular and physiological aspects of nitrate uptake in plants. *Trends in Plant Science, Reviews*, *3*(10), 389–395. https://doi.org/10.1016/s1360-1385(98)01311-9

Cushman, K. C., Bunyavejchewin, S., Cárdenas, D., Condit, R., Davies, S. J., Duque, A., et al. (2021). Variation in trunk taper of buttressed trees within and among five lowland tropical forests. *Biotropica*, *53*(5), 1442–1453. https://doi.org/10.1111/btp.12994

Dantas de Paula, M., Forrest, M., Langan, L., Bendix, J., Homeier, J., Velescu, A., et al. (2021). Nutrient cycling drives plant community trait assembly and ecosystem functioning in a tropical mountain biodiversity hotspot. *New Phytologist*, *232*(2), 551–566. https://doi.org/10.1111/nph.17600

de Kauwe, M. G., Medlyn, B. E., Zaehle, S., Walker, A. P., Dietze, M. C., Wang, Y.-P., et al. (2014). Where does the carbon go? A model–data intercomparison of vegetation carbon allocation and turnover processes at two temperate forest free-air CO_2 enrichment sites. *New Phytologist*, *203*(3), 883–899. https://doi.org/10.1111/nph.12847

Detto, M. (2022). Barro Colorado island - Eddy covariance flux data (2012–2017) [Dataset]. Dryad. https://doi.org/10.5061/dryad.3tx95x6j5

Edwards, J., Foucar, J., Mametjanov, A., Jacob, R., Sacks, B., singhbalwinder, et al. (2023). RGKNOX/E3SM: Manuscript release - Knox et al. 2023 [Software]. Zenodo. https://doi.org/10.5281/zenodo.7684977

Ely, K., Rogers, A., Serbin, S., Wu, J., Dickman, T., Collins, A., et al. (2019). Leaf mass area, Feb2016-May2016, PA-SLZ, PA-PNM, PA-BCI: Panama. 1.0. NGEE Tropics Data Collection [Dataset]. https://doi.org/10.15486/ngt/1411973

Fang, Y., Leung, L. R., Knox, R., Koven, C., & Bond-Lamberty, B. (2022). Impact of the numerical solution approach of a plant hydrodynamic model (v0.1) on vegetation dynamics. *Geoscientific Model Development*, *15*(16), 6385–6398. https://doi.org/10.5194/gmd-15-6385-2022

Farquhar, G., von Caemmerer, S., & Berry, J. (1980). A biochemical model of photosynthetic CO_2 assimilation in leaves of C_3 species. *Planta*, *149*(1), 78–90. https://doi.org/10.1007/BF00386231

Farrior, C. E., Tilman, D., Dybzinski, R., Reich, P. B., Levin, S. A., & Pacala, S. W. (2013). Resource limitation in a competitive context determines complex plant responses to experimental resource additions. *Ecology*, *94*(11), 2505–2517. https://doi.org/10.1890/12-1548.1

FATES-Development-Team. (2019). Technical note for the Functionally Assembled Terrestrial Ecosystem Simulator (FATES) [Technical Documentation]. *Zenodo*. https://doi.org/10.5281/zenodo.3517272

FATES-Development-Team. (2023). Fates software for ELM-FATES-CNP (with scripts) [Software]. Zenodo. https://doi.org/10.5281/zenodo.7685350

Faybishenko, B., Paton, S., Powell, T., Knox, R., Pastorello, G., Varadharajan, C., et al. (2018). QA/QC-ED BCI meteorological drivers. NGEE tropics data collection, NGT0062-v1 [Dataset]. https://doi.org/10.15486/ngt/1423307

Fisher, J., Sitch, S., Malhi, Y., Fisher, R., Huntingford, C., & Tan, S. (2010). A mechanistic, globally applicable model of plant nitrogen uptake, retranslocation, and fixation. *Global Biogeochemical Cycles*, *24*(1). https://doi.org/10.1029/2009GB003621

Fisher, R. A., Muszala, S., Verteinstein, M., Lawrence, P., Xu, C., McDowell, N. G., et al. (2015). Taking off the training wheels: The properties of a dynamic vegetation model without climate envelopes. *Geoscientific Model Development Discussions*, *8*(4), 3293–3357. https://doi.org/10.5194/gmdd-8-3293-2015

Forde, B., & Lorenzo, H. (2001). The nutritional control of root development. *Plant and Soil*, *232*(1/2), 51–68. https://doi.org/10.1023/A:1010329902165

Freschet, G., Cornelissen, J., van Logstestijn, R., & Aerts, R. (2010). Substantial nutrient resorption from leaves, stems and roots in subarctic flora: What is the link with other resource economics traits? *New Phytologist*, *186*(4), 879–889. https://doi.org/10.1111/j.1469-8137.2010.03228.x

Fyllas, N., Gloor, E., Mercado, L., Sitch, S., Quesada, C., Domingues, T., et al. (2014). Analysing Amazonian forest productivity using a new individual and trait-based model (TFS v. 1). *Geoscientific Model Development*, *7*(4), 1251–1269. https://doi.org/10.5194/gmd-7-1251-2014

Gaudinski, J. B., Torn, M. S., Riley, W. J., Dawson, T. E., Joslin, J. D., & Majdi, H. (2010). Measuring and modeling the spectrum of fine-root turnover times in three forests using isotopes, minirhizotrons, and the Radix model. *Global Biogeochemical Cycles*, *24*(3). https://doi.org/10.1029/2009GB003649

Hanbury-Brown, A. R., Ward, R. E., & Kueppers, L. M. (2022). Forest regeneration within earth system models: Current process representations and ways forward. *New Phytologist*, *235*(1), 20–40. https://doi.org/10.1111/nph.18131

Houlton, B., Wang, Y., Vitousek, P., & Field, C. B. (2008). A unifying framework for dinitrogen fixation in the terrestrial biosphere. *Nature*, *454*(7202), 327–330. https://doi.org/10.1038/nature07028

Hungate, B., Dukes, J., Shaw, M., Luo, Y., & Field, C. (2003). Nitrogen and climate change. *Science*, *302*(5650), 1512–1513. https://doi.org/10.1126/science.1091390

Iversen, C. M., McCormack, M. L., Powell, A. S., Blackwood, C. B., Freschet, G. T., Kattge, J., et al. (2017). A global fine-root ecology database to address below-ground challenges in plant ecology. *New Phytologist*, *215*(1), 15–26. https://doi.org/10.1111/nph.14486

Knox, R., Faybishenko, B., Paton, S., Powell, T., Pastorello, G., Koven, C., et al. (2019). Panama land model (CLM/ELM) site drivers, NGT0086-v1.0. [Dataset]. https://doi.org/10.15486/ngt/1570244

Kou-Giesbrecht, S., Malyshev, S., Martínez Cano, I., Pacala, S. W., Shevliakova, E., Bytnerowicz, T. A., & Menge, D. N. L. (2021). A novel representation of biological nitrogen fixation and competitive dynamics between nitrogen-fixing and non-fixing plants in a land model (GFDL LM4.1-BNF). *Biogeosciences*, *18*(13), 4143–4183. https://doi.org/10.5194/bg-18-4143-2021

Koven, C., Riley, W., Subin, Z., Tang, J., Torn, M., Collins, W., et al. (2013). The effect of vertically resolved soil biogeochemistry and alternate soil C and N models on C dynamics of CLM4. *Biogeosciences*, *10*(11), 7109–7131. https://doi.org/10.5194/bg-10-7109-2013

Koven, C. D., Knox, R. G., Fisher, R. A., Chambers, J. Q., Christoffersen, B. O., Davies, S. J., et al. (2020). Benchmarking and parameter sensitivity of physiological and vegetation dynamics using the Functionally Assembled Terrestrial Ecosystem Simulator (FATES) at Barro Colorado Island, Panama. *Biogeosciences*, *17*(11), 3017–3044. https://doi.org/10.5194/bg-17-3017-2020

Kyker-Snowman, E., Wieder, W. R., Frey, S. D., & Grandy, A. S. (2020). Stoichiometrically coupled carbon and nitrogen cycling in the Microbial-Mineral Carbon Stabilization model version 1.0 (MIMICS-CN v1.0). *Geoscientific Model Development*, *13*(9), 4413–4434. https://doi.org/10.5194/gmd-13-4413-2020

Lamour, J., Davidson, K. J., Ely, K. S., Le Moguédec, G., Anderson, J. A., Li, Q., et al. (2023). The effect of the vertical gradients of photosynthetic parameters on the CO_2 assimilation and transpiration of a Panamanian tropical forest. *New Phytologist*, *238*(6), 2345–2362. https://doi.org/10.1111/nph.18901

Lawrence, D., Fisher, R., Koven, C., Oleson, K., Swenson, S., Vertenstein, M., et al. (2020). *Technical description of version 5.0 of the community land model (CLM)*. Geoscientific Model Development. Retrieved from https://www2.cesm.ucar.edu/models/cesm2/land/CLM50_Tech_Note.pdf

LeBauer, D. S., Wang, D., Richter, K. T., Davidson, C. C., & Dietze, M. C. (2013). Facilitating feedbacks between field measurements and ecosystem models. *Ecological Monographs*, *83*(2), 133–154. https://doi.org/10.1890/12-0137.1

Lu, D., Ricciuto, D., Stoyanov, M., & Gu, L. (2018). Calibration of the E3SM land model using surrogate-based global optimization. *Journal of Advances in Modeling Earth Systems*, *10*(6), 1337–1356. https://doi.org/10.1002/2017MS001134

Ma, W., Zhai, L., Pivovaroff, A., Shuman, J., Buotte, P., Ding, J., et al. (2021). Assessing climate change impacts on live fuel moisture and wildfire risk using a hydrodynamic vegetation model. *Biogeosciences*, *18*(13), 4005–4020. https://doi.org/10.5194/bg-18-4005-2021

Mahowald, N., Jickells, T. D., Baker, A. R., Artaxo, P., Benitez-Nelson, C. R., Bergametti, G., et al. (2008). Global distribution of atmospheric phosphorus sources, concentrations and deposition rates, and anthropogenic impacts. *Global Biogeochemical Cycles*, *22*(4). https://doi.org/10.1029/2008GB003240

Martínez Cano, I., Muller-Landau, H. C., Wright, S. J., Bohlman, S. A., & Pacala, S. W. (2019). Tropical tree height and crown allometries for the Barro Colorado Nature Monument, Panama: A comparison of alternative hierarchical models incorporating interspecific variation in relation to life history traits. *Biogeosciences*, *16*(4), 847–862. https://doi.org/10.5194/bg-16-847-2019

McCormack, M. L., Dickie, I. A., Eissenstat, D. M., Fahey, T. J., Fernandez, C. W., Guo, D., et al. (2015). Redefining fine roots improves understanding of below-ground contributions to terrestrial biosphere processes. *New Phytologist*, *207*(3), 505–518. https://doi.org/10.1111/nph.13363

McMurtrie, R. E., & Näsholm, T. (2018). Quantifying the contribution of mass flow to nitrogen acquisition by an individual plant root. *New Phytologist*, *218*(1), 119–130. https://doi.org/10.1111/nph.14927

Medvigy, D., Wang, G., Zhu, Q., Riley, W. J., Trierweiler, A. M., Waring, B., et al. (2019). Observed variation in soil properties can drive large variation in modelled forest functioning and composition during tropical forest secondary succession. *New Phytologist*, *223*(4), 1820–1833. https://doi.org/10.1111/nph.15848

Menge, D. N. L., Wolf, A. A., Funk, J. L., Perakis, S. S., Akana, P. R., Arkebauer, R., et al. (2022). Tree symbioses sustain nitrogen fixation despite excess nitrogen supply. *Ecological Monographs*, *93*(2), e1562. https://doi.org/10.1002/ecm.1562

Millard, P., & Grelet, G.-A. (2010). Nitrogen storage and remobilization by trees: Ecophysiological relevance in a changing world. *Tree Physiology*, *30*(9), 1083–1095. https://doi.org/10.1093/treephys/tpq042

Mirabello, M. J., Yavitt, J. B., Garcia, M., Harms, K. E., Turner, B. L., & Wright, S. J. (2013). Soil phosphorus responses to chronic nutrient fertilisation and seasonal drought in a humid lowland forest, Panama. *Soil Research*, *51*(3), 215–221. https://doi.org/10.1071/SR12188

Moorcroft, P., Hurtt, G., & Pacala, S. W. (2001). A method for scaling vegetation dynamics: The ecosystem demography model. *Ecological Monographs*, *71*(4), 557–586. https://doi.org/10.1890/0012-9615(2001)071[0557:amfsvd]2.0.co;2

Muller-Landau, H., & Wright, S. J. (Eds.). (2023). *The first 100 years of research on Barro Colorado island: Plant and ecosystem science*. Smithsonian Institution Scholarly Press.

Nambiar, E. (1987). Do nutrients restranslocate from fine roots? *Canadian Journal of Forest Research*, *17*(8), 913–918. https://doi.org/10.1139/x87-143

Needham, J. F., Arellano, G., Davies, S. J., Fisher, R. A., Hammer, V., Knox, R. G., et al. (2022). Tree crown damage and its effects on forest carbon cycling in a tropical forest. *Global Change Biology*, *28*(18), 5560–5574. https://doi.org/10.1111/gcb.16318

Needham, J. F., Chambers, J., Fisher, R., Knox, R., & Koven, C. D. (2020). Forest responses to simulated elevated CO_2 under alternate hypotheses of size- and age-dependent mortality. *Global Change Biology*, *26*(10), 5734–5753. https://doi.org/10.1111/gcb.15254

Norman, J. (1979). *Modeling the complete crop canopy. Modification of the aerial environment of crops* (pp. 249–280). American Society Agricultural Engineers.

Oleson, K., Lawrence, D., Bonan, G., Drewniak, B., Huang, C., Koven, C., et al. (2013). *Technical description of version 4.5 of the community land model (CLM)*. Geoscientific Model Development.

Parton, W., Stewart, J., & Cole, C. (1988). Dynamics of C, N, P and S in grassland soils – A model. *Biogeochemistry*, *5*(1), 109–131. https://doi.org/10.1007/bf02180320

Patton, S. (2019a). Barro Colorado Island, Lutz tower 48m air temperature. Smithsonian tropical research institute [Dataset]. https://doi.org/10.25573/data.10042442.v24

Patton, S. (2019b). Barro Colorado Island, Lutz tower 48m relative humidity. Smithsonian tropical research institute [Dataset]. https://doi.org/10.25573/data.10042418.v23

Patton, S. (2019c). Barro Colorado Island, Lutz tower 48m solar radiation, Pyranometer. Smithsonian tropical research institute. [Dataset]. https://doi.org/10.25573/data.10042406.v20

Patton, S. (2019d). Barro Colorado Island, Lutz tower 48m wind speed. Smithsonian tropical research institute [Dataset]. https://doi.org/10.25573/data.10042427.v20

Pinnington, E., Quaife, T., Lawless, A., Williams, K., Arkebauer, T., & Scoby, D. (2020). The land variational ensemble data assimilation framework: Lavendar v1.0.0. *Geoscientific Model Development*, *13*(1), 55–69. https://doi.org/10.5194/gmd-13-55-2020

Poorter, H., Niklas, K. J., Reich, P. B., Oleksyn, J., Poot, P., & Mommer, L. (2012). Biomass allocation to leaves, stems and roots: Meta-analyses of interspecific variation and environmental control. *New Phytologist*, *193*(1), 30–50. https://doi.org/10.1111/j.1469-8137.2011.03952.x

Powers, J., Treseder, K., & Lerdau, M. (2005). Fine roots, arbuscular mycorrhizal hyphae and soil nutrients in four neotropical rain forests: Patterns across large geographic distances. *New Phytologist*, *165*(3), 913–921. https://doi.org/10.1111/j.1469-8137.2004.01279.x

Prentice, I., Liang, X., Medlyn, B., & Wang, Y.-P. (2015). Reliable, robust and realistic: The three R's of next-generation land-surface modelling. *Atmospheric Chemistry and Physics*, *15*(10), 5987–6005. https://doi.org/10.5194/acp-15-5987-2015

Purves, D., & Pacala, S. (2008). Predictive models of forest dynamics. *Science*, *320*(5882), 1452–1453. https://doi.org/10.1126/science.1155359

Purves, D. W., Lichstein, J. W., Strigul, N., & Pacala, S. W. (2008). Predicting and understanding forest dynamics using a simple tractable model. *Proceedings of the National Academy of Sciences*, *105*(44), 17018–17022. https://doi.org/10.1073/pnas.0807754105

Ryan, M. G. (1991). A simple method for estimating gross carbon budgets for vegetation in forest ecosystems. *Tree Physiology*, *9*(1–2), 255–266. https://doi.org/10.1093/treephys/9.1-2.255

Sinha, E., Calvin, K. V., Bond-Lamberty, B., Drewniak, B. A., Ricciuto, D. M., Sargsyan, K., et al. (2023). Modeling perennial bioenergy crops in the E3SM land model (ELMV2). *Journal of Advances in Modeling Earth Systems*, *15*(1), e2022MS003171. https://doi.org/10.1029/2022MS003171

Smith, B., Wärlind, D., Arneth, A., Hickler, T., Leadley, P., Siltberg, J., & Zaehle, S. (2014). Implications of incorporating n cycling and n limitations on primary production in an individual-based dynamic vegetation model. *Biogeosciences*, *11*(7), 2027–2054. https://doi.org/10.5194/bg-11-2027-2014

Steudle, E., & Peterson, C. A. (1998). How does water get through roots? *Journal of Experimental Botany*, *49*(322), 775–788. https://doi.org/10.1093/jxb/49.322.775

Sulman, B., Shevliakova, E., Brzostek, E., Kivlin, S., Malyshev, S., Menge, D., & Zhang, X. (2019). Diverse mycorrhizal associations enhance terrestrial C storage in a global model. *Global Biogeochemical Cycles*, *33*(4), 501–523. https://doi.org/10.1029/2018GB005973

Tang, J., & Riley, W. (2013). A total quasi-steady-state formulation of substrate uptake kinetics in complex networks and an example application to microbial litter decomposition. *Biogeosciences*, *10*(12), 8329–8351. https://doi.org/10.5194/bg-10-8329-2013

Taylor, B. N., Strand, A. E., Cooper, E. R., Beidler, K. V., Schönholz, M., & Pritchard, S. G. (2014). Root length, biomass, tissue chemistry and mycorrhizal colonization following 14 years of CO_2 enrichment and 6 years of n fertilization in a warm temperate forest. *Tree Physiology*, *34*(9), 955–965. https://doi.org/10.1093/treephys/tpu058

Thonicke, K., Spessa, A., Prentice, I., Harrison, S., Dong, L., & Carmona-Moreno, C. (2010). The influence of vegetation, fire spread and fire behaviour on biomass burning and trace gas emissions: Results from a process-based model. *Biogeosciences*, *7*(6), 1991–2011. https://doi.org/10.5194/bg-7-1991-2010

Thornley, J. (1995). Shoot: Root allocation with respect to C, N and P: An investigation and comparison of resistance and teleonomic models. *Annals of Botany*, *75*(4), 391–405. https://doi.org/10.1006/anbo.1995.1037

Thornton, P., Lamarque, J.-F., Rosenbloom, N., & Mahowald, N. (2007). Influence of carbon-nitrogen cycle coupling on land model response to CO_2 fertilization and climate variability. *Global Biogeochemical Cycles*, *21*(GB4018). https://doi.org/10.1029/2006gb002868

Thornton, P. E., Doney, S. C., Lindsay, K., Moore, J. K., Mahowald, N., Randerson, J. T., et al. (2009). Carbon-nitrogen interactions regulate climate-carbon cycle feedbacks: Results from an atmosphere-ocean general circulation model. *Biogeosciences*, *6*(10), 2099–2120. https://doi.org/10.5194/bg-6-2099-2009

Thornton, P. E., & Rosenbloom, N. A. (2005). Ecosystem model spin-up: Estimating steady state conditions in a coupled terrestrial carbon and nitrogen cycle model. *Ecological Modelling*, *189*(1–2), 25–48. https://doi.org/10.1016/j.ecolmodel.2005.04.008

Thum, T., Caldararu, S., Engel, J., Kern, M., Pallandt, M., Schnur, R., et al. (2019). A new model of the coupled carbon, nitrogen, and phosphorus cycles in the terrestrial biosphere (QUINCY v1.0; revision 1996). *Geoscientific Model Development*, *12*(11), 4781–4802. https://doi.org/10.5194/gmd-12-4781-2019

Walker, A., Beckerman, A., Gu, L., Kattge, J., Cernusak, L., Domingues, T., et al. (2014). The relationship of leaf photosynthetic traits - V_{cmax} and J_{max} - To leaf nitrogen, leaf phosphorus, and specific leaf area: A meta-analysis and modeling study. *Ecology and Evolution*, *4*(16), 3218–3235. https://doi.org/10.1002/ece3.1173

Wang, Y. P., Law, R. M., & Pak, B. (2010). A global model of carbon, nitrogen and phosphorus cycles for the terrestrial biosphere. *Biogeosciences*, *7*(7), 2261–2282. https://doi.org/10.5194/bg-7-2261-2010

Wang, Y.-P., Zhang, Q., Pitman, A., & Dai, Y. (2015). Nitrogen and phosphorous limitation reduces the effects of land use change on land carbon uptake or emission. *Environmental Research Letters*, *10*(1), 014001. https://doi.org/10.1088/1748-9326/10/1/014001

Wieder, R. K., & Wright, S. J. (1995). Tropical forest litter dynamics and dry season irrigation on Barro Colorado Island, Panama. *Ecology*, *76*(6), 1971–1979. https://doi.org/10.2307/1940727

Wieder, W. R., Sulman, B. N., Hartman, M. D., Koven, C. D., & Bradford, M. A. (2019). Arctic soil governs whether climate change drives global losses or gains in soil carbon. *Geophysical Research Letters*, *46*(24), 14486–14495. https://doi.org/10.1029/2019gl085543

Wright, S. J., Kitajima, K., Kraft, N. J. B., Reich, P. B., Wright, I. J., Bunker, D. E., et al. (2010). Functional traits and the growth–mortality trade-off in tropical trees. *Ecology*, *91*(12), 3664–3674. https://doi.org/10.1890/09-2335.1

Yang, S.-Y., Huang, T.-K., Kuo, H.-F., & Chiou, T.-J. (2017). Role of vacuoles in phosphorus storage and remobilization. *Journal of Experimental Botany*, *68*(12), 3045–3055. https://doi.org/10.1093/jxb/erw481

Yang, X., Ricciuto, D., Thornton, P., Shi, X., Xu, M., Hoffman, F., & Norby, R. (2019). The effects of phosphorus cycle dynamics on carbon sources and sinks in the amazon region: A modeling study using ELM v1. *Journal of Geophysical Research: Biogeosciences*, *124*(12), 3686–3698. https://doi.org/10.1029/2019JG005082

Yang, X., Thornton, P., Ricciuto, D., & Post, W. (2014). The role of phosphorus dynamics in tropical forests-a modeling study using CLM-CNP. *Biogeosciences*, *11*(6), 1667–1681. https://doi.org/10.5194/bg-11-1667-2014

Yang, X., Wm, P., Thornton, P., & Jain, A. (2013). The distribution of soil phosphorus for global biogeochemical modeling. *Biogeosciences*, *10*(4), 2525–2537. https://doi.org/10.5194/bg-10-2525-2013

Yavitt, J., Harms, K., Garcia, M., Mirabello, M., & Wright, S. (2011). Soil fertility and fine root dynamics in response to 4 years of nutrient (N, P, K) fertilization in a lowland tropical moist forest, Panama. *Austral Ecology*, *36*, 433–445. https://doi.org/10.1111/j.1442-9993.2010.02157.x

Yavitt, J., & Wright, S. (2001). Drought and irrigation effects on fine root dynamics in a tropical moist forest, Panama. *Biotropica*, *33*(3), 421–434. https://doi.org/10.1646/0006-3606(2001)033[0421:DAIEOF]2.0.CO;2

Zaehle, S., & Friend, A. (2010). Carbon and nitrogen cycle dynamics in the O-CN land surface model: 1. Model description, site-scale evaluation, and sensitivity to parameter estimates. *Global Biogeochemical Cycles*, *24*(1). https://doi.org/10.1029/2009gb003521

Zhu, Q., Riley, W., Tang, J., Collier, N., Hoffman, F., Yang, X., & Bisht, G. (2019). Representing nitrogen, phosphorus, and carbon interactions in the E3SM land model: Development and global benchmarking. *Journal of Advances in Modeling Earth Systems*, *11*(7), 2238–2258. https://doi.org/10.1029/2018MS001571

Zhu, Q., Riley, W., Tang, J., & Koven, C. (2016). Multiple soil nutrient competition between plants, microbes, and mineral surfaces: Model development, parameterization, and example applications in several tropical forests. *Biogeosciences*, *12*(5), 4057–4106. https://doi.org/10.5194/bgd-12-4057-2015